Research Square

Preprints are preliminary reports that have not undergone peer review.
They should not be considered conclusive, used to inform clinical practice,
or referenced by the media as validated information.

Copper oxide nanoparticles show pathogen-dependent activity against grapevine trunk disease-associated fungi and modulate grapevine defence responses

Jana Čechová
Mendel University in Brno
Kateřina Štůsková
Mendel University in Brno
Tomáš Kiss
Mendel University in Brno
Lucie Frejlichová
Mendel University in Brno
Jana Pekárková
Mendel University in Brno
Eliška Birgusová
Mendel University in Brno
Andrea Ridošková
Mendel University in Brno
Lukáš Richtera
Mendel University in Brno
David Gramaje
Instituto de Ciencias de la Vid y del Vino (ICVV), Spanish National Research Council (CSIC), University of La Rioja and Government of La Rioja
Aleš Eichmeier
ales.eichmeier@mendelu.cz

Mendel University in Brno

Research Article

Keywords: Nanoparticles, trunk diseases, antifungal activity, plant protection, gene expression, stilbene synthase, chitinase, sustainable agriculture

Posted Date: November 25th, 2026

DOI: https://doi.org/10.21203/rs.3.rs-11615899/v1

License: This work is licensed under a Creative Commons Attribution 4.0 International License.
Read Full License

Additional Declarations: No competing interests reported.

Copper oxide nanoparticles show pathogen-dependent activity against grapevine trunk disease-associated fungi and modulate grapevine defence responses

Jana Čechová[1], Kateřina Štůsková[1], Tomáš Kiss[1], Lucie Frejlichová[1], Jana Pekárková[2,3], Eliška Birgusová[2], Andrea Ridošková[2], Lukáš Richtera[2], David Gramaje[4], Aleš Eichmeier[1]

[1]Mendeleum - Institute of Genetics, Faculty of Horticulture, Mendel University in Brno, 61300 Brno, Czech Republic

[2]Department of Chemistry and Biochemistry, Mendel University in Brno, 61300 Brno, Czech Republic

[3]Department of Microelectronics, Faculty of Electrical Engineering and Communication, Brno University of Technology, 616 00 Brno, Czech Republic

[4]Instituto de Ciencias de la Vid y del Vino (ICVV), Spanish National Research Council (CSIC), University of La Rioja and Government of La Rioja, 26007 Logroño, Spain

Correspondence: A. Eichmeier, ales.eichmeier@mendelu.cz

ABSTRACT

Background

Grapevine trunk diseases (GTDs) pose a major challenge to sustainable viticulture, while effective control strategies remain limited. Copper oxide nanoparticles (CuO NPs) represent a potential alternative for suppressing fungal pathogens, although their efficacy against GTD-associated fungi and their effects on grapevine defence responses remain insufficiently

understood. This study evaluated the antifungal activity of CuO NPs and their graphene oxide (GO-CuO) and reduced graphene oxide (rGO-CuO) composites, together with the effects of selected CuO formulations on wood necrosis and defence-related gene expression in grapevine.

Results

In vitro assays revealed pronounced pathogen-dependent antifungal activity, with CuO NPs consistently outperforming graphene-modified formulations. The strongest growth inhibition was observed against *Fomitiporia mediterranea*, whereas *Diplodia seriata* and *Neonectria* sp. showed comparatively high tolerance. Under *in planta* conditions, the effects of CuO NPs on wood necrosis varied according to the pathogen and formulation. Two CuO formulations significantly reduced wood necrosis caused by *D. torresensis* and *F. oxysporum*, whereas only one formulation was effective against *P. richardsiae*. Analysis of defence-related gene expression revealed pathogen-dependent responses, including the upregulation of *VvSTS* and *VvChit4c*, suggesting the involvement of stilbene biosynthesis and chitinase-associated defence pathways.

Conclusions

CuO NPs exhibit pathogen-dependent antifungal activity and can reduce wood necrosis caused by selected GTD-associated fungi under controlled conditions. Their effects on grapevine defence-related gene expression further suggest a potential contribution of host responses to disease suppression. These findings support further investigation of CuO-based formulations as targeted tools for grapevine trunk disease management, including validation under nursery and vineyard conditions.

KEYWORDS

Nanoparticles, trunk diseases, antifungal activity, plant protection, gene expression, stilbene synthase, chitinase, sustainable agriculture

INTRODUCTION

Currently, agriculture represents the largest interface between humans and the environment and is simultaneously the main driver of soil and ecosystem modification [1,2]. These modifications are primarily achieved using chemical compounds; nevertheless, crop yield losses caused by pathogens, pests, and weeds remain high, accounting for 20–50 % of global agricultural production [2–4]. However, pathogens are gradually developing resistance to these chemicals, which may also damage the environment and pose risks to human and animal health [5,6]. In addition, chemicals are extensively used as fertilizers, which are often applied inefficiently and wastefully [2]. In the context of efforts to reduce the reliance on chemical inputs in agriculture, nanoparticles (NPs) represent a highly promising alternative [7]. For example, the encapsulation of active substances within NPs enables their improved and sustained delivery to soil and plants, while reducing their toxicity compared to their free form. Moreover, due to their highly reactive surface, NPs themselves are biologically active and can be employed as fertilizers, plant growth stimulators, pesticides, or carriers for conventional pesticides [2,8–10].

Various NPs have been evaluated as nanopesticides, and numerous studies demonstrate that NPs exhibit significant antifungal and antibacterial activities in both *in vitro* and *in planta* experiments. For example, sulfur NPs have been shown to inhibit the growth of *Aspergillus niger* van Tieghem, 1867 and *Fusarium oxysporum* Schltdl. under *in vitro* conditions [11,12]. Gold NPs (Au NPs) functionalized with mercaptoimidazole exhibited *in vitro* inhibition of the pathogens *Magnaporthe oryzae* B.C.Couch, *Botrytis cinerea* Pers., *Fusarium pseudograminearum* O'Donnell & T.Aoki, and *Colletotrichum destructivum* O'Gara. In pot

experiments, these NPs significantly reduced the incidence of *B. cinerea* infection on *Arabidopsis thaliana* (L.) Heynh. from 74.6 % to 6.2 %, and on *Solanum lycopersicum* L. from 100 % to 10.9 % [13]. An inhibition rate of 87.43 % against *Colletotrichum capsici (*Syd. & P.Syd.) E.J.Butler & Bisby, the causal agent of chili anthracnose, was also observed for Au NPs. Furthermore, Au NPs reduced disease incidence on chili peppers (*Capsicum annum* L.) from 79 % in control plants to 23 % in treated plants [14]. Numerous studies have also confirmed the inhibitory effects of silver [15–21], nickel [22–24], platinum [25,26], zinc [18,20,27,28], titanium [20], graphene- [28,29], chitosan- [23,30,31], and copper-based [18,32,33] NPs. Collectively, these findings demonstrate a highly promising alternative approach for the protection of grapevines against fungal pathogens associated with the GTDs complex.

In 2024, grapevines were cultivated worldwide on 6.73 million hectares, with an average yield of 11,000 kg ha^{-1} and a total production of 76 million tonnes of grapes (FAOSTAT, 2024), of which approximately 71 % is used for wine production, 27 % for fresh consumption, and 2 % as dried fruit, underscoring the critical global economic importance of this crop [35]. In the context of ongoing climate change, GTDs are emerging as one of the most severe and rapidly escalating threats to viticulture, caused by fungal pathogens belonging to nine distinct families [36]. GTDs comprise six major diseases: Esca, Eutypa dieback, Phomopsis dieback, Botryosphaeria dieback, Petri disease, and Black foot disease. The first four primarily affect grapevine trunks older than five years, whereas Petri disease and Black foot disease predominantly infect young grapevine planting material and nursery vines [37–39]. These diseases manifest a broad spectrum of symptoms, including internal wood discoloration and necrosis in both perennial wood and current-year shoots, leading to vascular dysfunction and impaired transport of water and nutrients. Aboveground symptoms include leaf and fruit damage, which collectively result in reduced photosynthetic capacity, significant yield losses,

and the progressive dieback of shoots, canes, spurs and ultimately entire grapevine plants [38–41].

Control strategies against these diseases are highly limited, particularly following the ban on sodium arsenite due to its severe adverse effects on human health and the environment [36]. Consequently, current management relies predominantly on preventive measures, including symptom monitoring and the removal of infected vines [39,42]. Moreover, increasing efforts to reduce the use of chemical inputs have driven the search for alternative approaches, ranging from biological control strategies, such as the application of mycoparasitic fungi, notably *Trichoderma* spp. [43,44], to physical methods like hot water treatment [38,45], as well as the evaluation of NPs as potential agents against GTD-associated pathogens.

In *in vitro* assays, the inhibitory activity of a silver–selenium nanocomposite (AgSe NPs) and selenium NPs (Se NPs) was demonstrated against three GTD pathogens, namely *Eutypa lata* (Pers.) Tul. & C.Tul., *Diplodia seriata* De Not., and *Diaporthe eres* Nitschke. In contrast, a copper–selenium nanocomposite (CuSe NPs), as well as silver NPs (Ag NPs) and copper NPs (Cu NPs), significantly inhibited only *E. lata* among the three tested pathogens [46]. Furthermore, AgSe NPs were evaluated *in planta*, where they exhibited a significant inhibitory effect against *D. eres* and *E. lata*, but not against *D. seriata*. These findings indicate a pathogen-dependent efficacy of the tested NPs and highlight the strong potential of AgSe NPs for targeted control of selected GTD-associated fungi [47]. CuO NPs, investigated in the present study, have previously been reported to exert pronounced antifungal activity against *A. niger* and *Alternaria alternata* (Fr.) Keissl., pathogens responsible for lesion development on photosynthetic tissues, grape berries, stems, and young leaves under field conditions in Mexico [48]. Despite these promising findings, the antifungal potential of CuO NPs against pathogens associated with GTDs remains unexplored, representing a significant gap in current knowledge. Therefore,

evaluating CuO NPs in the context of GTDs is essential to assess their potential as sustainable control agents.

Here, we provide the first comprehensive evaluation of CuO-based NPs against GTD-associated pathogens. Specifically, the objectives of this study were to: (i) synthesize CuO NPs and CuO NPs combined with graphene oxide (GO-CuO NPs) or reduced graphene oxide (rGO-CuO NPs); (ii) assess their inhibitory effects against selected GTD pathogens under *in vitro* conditions; (iii) select the most effective NPs based on *in vitro* performance and evaluate their efficacy under *in planta* conditions; and (iv) characterize the gene expression profiles of treated grapevine seedlings.

MATERIAL AND METHODS

Synthesis of nanomaterials for inhibition experiments

The nanomaterials rGO-CuO NPs, GO-CuO NPs, and CuO NPs were fabricated at the Department of Chemistry and Biochemistry, Mendel University in Brno. The synthesis of GO and rGO has been described previously [49]. CuO NPs were prepared by dissolving 3 g of copper(II) chloride ($CuCl_2$, Sigma Aldrich, St. Louis, MO, USA) in 160 mL of absolute ethanol (Penta, Prague, Czech Republic), while 1.8 g of sodium hydroxide (NaOH, Penta, Prague, Czech Republic) was dissolved in 50 mL of absolute ethanol. The NaOH solution was added dropwise to the $CuCl_2$ solution using a peristaltic pump at a flow rate of 0.25 mL min^{-1} under continuous magnetic stirring (250 rpm). The resulting precipitate was washed once with ethanol followed by three times with ultrapure water (18.2 MΩ·cm at 25 °C; Barnstead GenPure, Thermo Fisher Scientific, Langenselbold, Germany), dried overnight at 60 °C in a drying oven, and subsequently calcined at 200, 300 or 400 °C for 2 h at a heating rate of 3 °C min^{-1}.

GO-CuO and rGO-CuO nanocomposites were subsequently prepared using the synthesized CuO NPs. Briefly, 40 mg of GO (or rGO) was dispersed in 40 mL of ultrapure water and

sonicated for 30 min. Subsequently, 500 mg of CuO NPs was added, and the suspension was sonicated at 40 °C for an additional 30 min. Thereafter, 1 mL of 25% aqueous ammonia solution (NH_3 (aq.), Lach-Ner, Neratovice, Czech Republic) was added, and the mixture was sonicated for 60 min at 40 °C. The resulting suspension was washed four times with ultrapure water and dried overnight at 60 °C in a drying oven.

All three nanomaterials were prepared in three formulations differing only in the calcination temperature of the CuO NPs (200, 300 and 400 °C). The calcination temperature, Cu content of the NPs, Cu concentration in the stock suspensions (100 mg L^{-1} prepared in sterile ultrapure water) and the concentrations used in the *in vitro* inhibition assays are summarized in Table 1.

Characterization of nanomaterials

Scanning electron microscopy (SEM)

The morphology of the samples was examined by SEM. NPs suspensions were diluted 1:100 with ultrapure water, drop-cast onto silicon wafers, and allowed to dry at room temperature (20–25 °C). Images of GO-CuO and rGO-CuO nanocomposites were acquired using a MAIA3 SEM (TESCAN, Brno, Czech Republic) equipped with an in-beam secondary electron detector, operated at an accelerating voltage of 5.0 kV, a working distance of 2–3 mm, and magnifications ranging from 50,000× to 100,000×. The morphology of CuO NPs was analysed using a high-resolution Verios 460L SEM (Thermo Fisher Scientific, Waltham, MA, USA). Images were acquired at an accelerating voltage of 5 kV, a working distance of 4 mm, and a dwell time of 0.3 μs $pixel^{-1}$ using an in-lens secondary electron detector in immersion mode.

X-ray powder diffraction (XRD)

The crystalline phases of the prepared NPs were identified by XRD using a SmartLab 3 kW diffractometer (Rigaku Corporation, Tokyo, Japan) equipped with Cu Kα radiation (λ = 0.154

nm) and operated in Bragg-Brentano geometry. Diffraction patterns were collected over a 2θ range of 10–100° with a step size of 0.02° at a scanning speed of 4° min^{-1}, using an operating voltage of 40 kV and a current of 30 mA. The obtained diffraction patterns were analyzed with Rigaku PDXL2 software.

X-ray photoelectron spectroscopy (XPS)

The surface chemical composition and chemical states of the nanocomposites were analyzed by XPS using a Kratos Axis Supra spectrometer (Kratos Analytical, Manchester, UK) equipped with a monochromatic Al K_α X-ray source. Measurements were performed in hybrid lens mode at an emission current of 15 mA. High-resolution spectra were acquired with a pass energy of 20 eV. Peak fitting was carried out in CasaXPS software (version 2.3.27) using mixed Gaussian-Lorentzian line shapes. Charge neutralization was applied during the measurements. All binding energies were referenced to the C 1s peak at 284.8 eV, and the spectral background was subtracted using either the Shirley or Tougaard algorithm.

Raman spectroscopy

A Renishaw InVia Raman microscope (Renishaw, Gloucestershire, UK) was used to collect the Raman spectra. A laser beam with a wavelength of 633 nm was used to excite the molecules, and 0.75 mW of laser energy (50% of 15 mW) was used. The sample surfaces were investigated via a 50 × L objective. The time of exposure was 25 s of each point and 5 ecquistion points of each sample were collected and further analysed in Renishaw WiRE software version 5.2. After averaging, normalizing, and smoothing the spectra, the bands were identified by subtracting the baselines.

Determination of the Cu concentrations by atomic absorption spectrometry (AAS)

Before determining Cu content by atomic absorption spectrometry (AAS), the graphene oxide-based NPs were subjected to microwave-assisted digestion. 0.1 mL of each sample was mixed with 5.0 mL of suprapure HNO_3 (70%, Merck, Darmstadt, Germany) and 5.0 mL of Milli-Q water. Digestion was performed using an Ethos ONE microwave system (Milestone, Sorisole, Italy) at 210 °C for 30 min. The digestion procedure was repeated twice, after which the sample was sonicated for 20 min in the ultrasonic bath (Elma Schmidbauer GmbH, Singen (Hohentwiel), Germany). Samples of CuO NPs were diluted 100× with 35% HNO_3. The Cu content in the prepared samples was determined using a 240 FS AA atomic absorption spectrometer (Agilent Technologies, Santa Clara, CA, USA) equipped with flame atomization and an acetylene–air flame. Calibration solutions were prepared from a Cu standard solution (1000 mg L^{-1}; Merck, Darmstadt, Germany) and acidified to a final concentration of 1 wt% HNO_3 using concentrated suprapure HNO_3. All solutions were prepared with demineralized water obtained from a Milli-Q purification system (Millipore, Bedford, MA, USA). Cu absorbance was measured at a wavelength of 324.8 nm.

Fungal isolates

For the *in vitro* inhibition assays, ten fungal species associated with GTDs were selected (abbreviations used are indicated in square brackets after the name): *Botryosphaeria dothidea* (Moug.) Ces. & De Not. [BD], *Dactylonectria torresensis* (A.Cabral, Rego & Crous) L.Lombard & Crous [DT], *Diaporthe ampelina* (Berk. & M.A.Curtis) R.R.Gomes, Glienke & Crous [DA], *D. seriata* [DS], *E. lata* [EL], *Fomitiporia mediterranea* M.Fisch. [FM], *F. oxysporum* [FO], *Neonectria* sp. Wollenw. [Ne], *Phaeoacremonium minimum* (Tul. & C.Tul.) Gramaje, L.Mostert & Crous [PM], and *Pleurostoma richardsiae* (Nannf.) L.Mostert, W.Gams & Crous [PR]. All isolates are included in the collection at the Mendeleum – Institute of Genetics, Mendel University in Brno (Lednice, Czech Republic). Further details of the isolates are provided in Table 2.

Inhibitory activity (*in vitro*)

In vitro experiment of inhibitory activity was performed following the methodology described by Štůsková *et al.* (2022) [46]. Stock suspensions of newly synthesized CuO NPs, GO-CuO NPs, and rGO-CuO NPs were prepared by dispersing 100 mg of NPs in 1 L of sterile water. The stock suspensions were used either undiluted or diluted 10-fold and 100-fold (Table 1). Seven days before the experiment, cultures of the selected GTD-associated fungal pathogens (Table 2) were established on potato dextrose agar (PDA; HiMedia, Čaderský-Envitek, Brno, Czech Republic) and incubated at 25 °C in the dark. The inhibition assay was performed on PDA plates (90 mm diameter) containing 20 mL of medium. After solidification of the medium, 100 µL of the NP suspension was applied to each plate (final concentration 5 µL NP suspension per 1 mL of medium) and even spread across the surface using a sterile microbiological loop. Mycelial plugs (5 mm in diameter) were excised from the actively growing margins of the fungal cultures using a sterile corkborer and placed in the center of each Petri dish. The plates were sealed with PARAFILM® M laboratory sealing film (Amcor Flexibles North America, Neenah, WI, USA), incubated in the dark at 25 °C, and monitored daily. Fungal growth was measured every day for 10 days using a ruler with millimeter resolution, recording colony radius at four positions between the edge of the inoculation plug and the colony margin. Negative control plates received sterile water instead of NP suspension, whereas positive control plates were treated with the commercially available fungicide Tessior (BASF SE, Ludwigshafen am Rhein, Germany), which contains boscalid (10 g L^{-1}; 0.95% w/w) and pyraclostrobin (5 g L^{-1}; 0.48% w/w). All treatments, including negative and positive controls, were established in three replicates. The percentage of inhibition was calculated according to the following formula: $I = \frac{(r_c - r_t)}{r_c} \times 100$, where I represents the percentage of inhibition, r_c the mean value recorded in the control treatment, and r_t the mean value recorded in the treated variant [50]. The values of r_c and r_t represent the mean radial growth calculated from all

measurements collected during the 10-day incubation period, yielding a single inhibition value for each treatment. To facilitate the visualization and comparison of antifungal activity across NP formulations and fungal pathogens, a heatmap was generated using ClustVis [51]. For treatments showing statistically significant inhibition, apparent half maximal effective concentration (EC_{50}) values, defined as the concentration causing 50% inhibition, were estimated using linear regression analysis based on the relationship between percentage inhibition and log-transformed NP concentration according to the equation: $y = a \times \log_{10}(x) + b$, where y represents the percentage inhibition (%), x NP concentration, a slope of the regression line and b intercept of the regression line. The EC_{50} values were subsequently calculated using the equation: $EC_{50} = 10^{\frac{50-b}{a}}$. Linear regression analysis was performed only for treatments showing a concentration-dependent decrease in inhibition with decreasing NP concentration. Treatments exhibiting irregular dose–response patterns, including lower inhibition at higher concentrations, were excluded from EC_{50} estimation, as such responses likely reflect additional factors affecting NP activity beyond a simple concentration-dependent effect. Due to the limited number of tested concentrations, the obtained EC_{50} values should be considered approximate estimates and interpreted with caution.

Inhibitory activity (*in planta*)

Based on the results of the *in vitro* assays, the most effective NPs were selected for *in planta* evaluation. Specifically, CuO NPs calcinated at 200, 300 and 400 °C (CuO-L-7, CuO-L-9 and CuO-L-3, respectively; Table 1) were used at a 10-fold dilution of the stock suspension. Three GTD-associated pathogens were included in the experiment: *D. torresensis*, *F. oxysporum*, and *P. richardsiae*. Fungal cultures were prepared seven days before inoculation and incubated in the dark at 25 °C. The grapevine cultivar Sauvignon Blanc, grafted onto rootstock SO4, was selected due to its high susceptibility to GTD pathogens [52]. The experiment was established in April 2022 in a net house at the Mendeleum – Institute of Genetics, Mendel University in

Brno (Lednice, Czech Republic). To assess the inhibitory effect of NPs under *in planta* conditions, the roots of each seedling were trimmed to approximately 8 cm from the base of the rootstock. The seedlings were then immersed in suspensions of the selected CuO NPs and hydrated for 24 h before planting, while tap water was used as the control treatment. Following hydration, an inoculation site was prepared at the root collar by creating a 3 mm diameter wound in the woody tissue using a sterile corkborer. A 3 mm mycelial plug, excised from the margin of an actively growing culture, was then placed onto the exposed wood surface. Each pathogen–treatment combination, including the control, consisted of five replicates. The inoculation site was covered with moistened cotton and sealed with PARAFILM® M to maintain suitable humidity and temperature conditions for pathogen development. The plants were subsequently transplanted into containers and maintained in the net house under regular monitoring and irrigation as required. After six months, plants were removed from the containers, washed with tap water, and evaluated for growth parameters, including total plant height (trunk height plus the length of the longest shoot) and root length. Wood necrosis was assessed by removing the bark at the inoculation site and measuring the length of necrotic tissue. Necrosis was expressed as a percentage of trunk height according to the following formula: $x = \frac{n}{s} \times 100$, where x represents the percentage of necrosis, n the length of necrotic tissue (cm), and s the trunk height (cm). Pathogens were re-isolated from the margins of necrotic tissues to confirm infection. Subsequently, RNA was extracted from wood tissues for gene expression analysis. The percentage inhibition of wood necrosis was calculated using the same formula as that applied in the *in vitro* experiment.

Re-isolation and molecular identification of pathogens

Necrotic wood tissues collected from the seedlings were surface-sterilized by briefly immersing them in absolute ethanol followed by flame sterilization. The tissues were then aseptically cut into small fragments using a sterile scalpel. The fragments were placed onto

Petri dishes containing PDA supplemented with streptomycin (100 mg L^{-1}; HiMedia, Čaderský-Envitek, Brno, Czech Republic) to suppress bacterial growth. Emerging fungal colonies were subcultured by transferring small pieces of mycelium onto fresh PDA plates to obtain pure cultures. Based on morphological characteristics, the isolates were classified into three groups corresponding to the genera *Dactylonectria*, *Fusarium*, and *Pleurostoma*. One representative isolate from each group was selected for molecular identification. Genomic DNA was extracted from the selected cultures using the NucleoSpin Tissue Kit (Macherey-Nagel, Düren, Germany). The internal transcribed spacer (ITS) region was amplified using the universal fungal primers ITS1 5′-TCC GTA GGT GAA CCT GCG G-3′ and ITS4 5′-TCC TCC GCT TAT TGA TAT GC-3′ [53]. Sequencing libraries were prepared using the Mix2Seq Kit (Eurofins Genomics, Ebersberg, Germany), and sequencing was performed by Eurofins Genomics. The obtained sequences were compared with reference sequences using the BLAST algorithm [54] against the NCBI GenBank database to confirm the taxonomic identity of the re-isolated fungi.

Gene expression profiling

To further elucidate the interaction between the pathogen, the host plant, and the applied NPs, the plant molecular response was investigated through gene expression profiling. Four defense-related marker genes were selected: pathogenesis-related protein 1 (VvPR1), non-expresser of pathogenesis-related gene 1 (VvNPR1), stilbene synthase (VvSTS), and acidic class IV chitinase (VvChit4c). The actin (VvACT) gene was used as the internal reference to normalize the expression levels of the target genes. This gene has been used as an internal reference in several other works [55,56]. Total RNA was isolated using the Spectrum™ Plant Total RNA Kit (Sigma-Aldrich, St. Louis, MO, USA). RNA concentration was measured with a SpectrostarNano spectrophotometer (BMG Labtech, Ortenberg, Germany) and adjusted to 90 ng μL^{-1} using nuclease-free water (Ambion, Pleasanton, CA, USA). Complementary DNA

(cDNA) was synthesized using the RevertAid RT Reverse Transcription Kit (Thermo Fisher Scientific, Waltham, MA, USA) following the protocol described by Eichmeier *et al.* (2010) [57]. Gene expression levels were quantified by quantitative real-time PCR (qPCR) using Genaxxon Mastermix (Genaxxon Bioscience GmbH, Ulm, Germany) on a qTower3 real-time PCR system (Analytik Jena, Jena-Göschwitz, Germany). Primer sequences used for amplification are listed in Table 3, while gene-specific thermal cycling conditions, PCR efficiencies and PCR product melting temperatures (T_m) of each amplified gene are provided in Table S1. Fluorescence detection and data processing were performed using qPCRsoft 3.4 software (Analytik Jena, Jena-Göschwitz, Germany). Normalized expression was calculated using delta delta Ct method with efficiency correction of each gene according to Pffafl (2001) [58] in the same qPCRsoft 3.4 software.

Statistical analysis

Statistical analyses were performed using Statistica 14 CZ (StatSoft, Prague, Czech Republic) and Python 3.13.2 (Python Software Foundation, Fredericksburg, VA, USA). All analyses were conducted separately for each pathogen, with statistical significance defined as $p < 0.05$.

For the *in vitro* experiments, the percentage inhibition of mycelial growth was used as the response variable. The normality of residuals was assessed using the Shapiro–Wilk test, which revealed no significant deviations from normality in any of the *in vitro* datasets ($p > 0.05$). Differences among treatments were subsequently evaluated using one-way analysis of variance (ANOVA), followed by the least significant difference (LSD) post hoc test. Each nanoparticle (NP) treatment was compared exclusively with the negative control (sterile water).

For the *in planta* experiment, grapevine height (cm), root length (cm), and the percentage of wood necrosis relative to trunk height (%) were evaluated separately for each pathogen, with

five biological replicates per treatment (n = 5). Normalized gene expression data obtained by quantitative PCR (qPCR) were analysed separately for each pathogen and target gene. For both datasets, the normality of residuals and homogeneity of variances were assessed using the Shapiro–Wilk and Levene's tests, respectively. When both assumptions were satisfied, treatment effects were evaluated using one-way ANOVA, followed by Dunnett's post hoc test. When residuals were normally distributed but homogeneity of variances was violated, Welch's ANOVA was applied, followed by two-sided Welch's t-tests with Holm's adjustment for multiple comparisons. When the assumption of normality was violated, the nonparametric Kruskal–Wallis test was employed, followed by Dunn's pairwise comparisons with Holm's adjustment. For both experiments, treatment-to-control contrasts were specified a priori and evaluated independently of the statistical significance of the overall omnibus test. All post hoc comparisons were restricted to individual NP treatments versus the corresponding negative control (tap water); comparisons among individual NP treatments were not performed. Statistical significance was defined as $p < 0.05$. In addition to statistical significance, biological changes in gene expression were interpreted relative to the corresponding controls: genes exhibiting a ≥2-fold increase in normalized expression were considered upregulated, whereas those showing a ≤0.5-fold change were considered downregulated.

To further assess the direction and magnitude of treatment specific effects on defence related gene expression, ordinary least squares (OLS) regression models were fitted separately for each pathogen. Log_{10}-transformed normalized gene expression values were used as the dependent variable, while treatment, target gene, and their interaction were included as explanatory variables. Because multiple gene expression measurements originated from the same plant sample, cluster robust standard errors were calculated at the plant sample level. Gene specific treatment contrasts were subsequently estimated relative to the corresponding untreated control and visualized as coefficient heatmaps [59].

RESULTS

Synthesis and characterization of nanomaterials

The morphology of CuO, GO-CuO and rGO-CuO prepared at different calcination temperatures was investigated by SEM (Figure 1). The pristine CuO samples (Figure 1A–C) consisted of nearly spherical NPs with dimensions of approximately 30–38 nm, as estimated from the SEM micrographs. With increasing calcination temperature, the particles became more regular and exhibited a more pronounced spherical morphology. NPs appeared as partially agglomerated clusters, which may be influenced by sample preparation for SEM analysis. In the GO-CuO composites (Figure 1D–F), CuO NPs were distributed on the surface of GO sheets while preserving the characteristic layered morphology of GO. The CuO NPs remained attached to both the basal planes and edges of the graphene sheets over the entire temperature range. The morphology of rGO-CuO (Figure 1G–I) differed from that of GO-CuO. A more folded and wrinkled structure was observed for rGO, resulting in a denser morphology. CuO NPs remained distributed across the rGO support, while their morphology became more regular with increasing calcination temperature.

XRD analysis confirmed the successful formation of crystalline CuO in all synthesized samples (Figure 2). The major diffraction peaks were indexed to monoclinic CuO (tenorite, ICSD 67850), consistent with previous reports [60], demonstrating that incorporation of GO and rGO did not alter the crystal structure of CuO. With increasing calcination temperature from 200 to 400 °C, the CuO diffraction peaks became progressively narrower and more intense, indicating increased crystallinity and an increase in the size of the coherent crystallite domains, as commonly reported for thermally treated CuO NPs [61,62]. A weak additional reflection at 16° (2θ) was observed in all pristine CuO samples. Its intensity decreased with increasing calcination temperature and was most pronounced in the sample calcined at 200 °C.

In contrast, this reflection was not detected in the GO-CuO and rGO-CuO nanocomposites [63]. No other distinct crystalline phases were detected.

Following the XRD, XPS was employed to investigate the surface chemical composition and oxidation states of CuO, GO-CuO and rGO-CuO nanocomposites. Since the spectra recorded for samples calcined at 200, 300 and 400 °C exhibited comparable spectral features without significant changes in the oxidation state of copper or the overall surface chemistry, only the spectra of the samples calcined at 400 °C are presented in Figure 3 as representative examples.

The high-resolution Cu 2p spectra of CuO-L-3 (Figure 3A), GO-CuO-L-3 (Figure 3C) and rGO-CuO-L-3 (Figure 3E) were deconvoluted into two Cu 2p spin–orbit doublets accompanied by the characteristic shake-up satellite peaks of Cu(II). The main Cu $2p_{3/2}$ component was centered at 933.52 eV (CuO-L-3), 934.56 eV (GO-CuO-L-3), and 933.65 eV (rGO-CuO-L-3), while the corresponding Cu $2p_{1/2}$ component appeared at 953.27, 954.31, and 953.40 eV, respectively. Additional fitted components were detected at 935.21/954.96 eV (CuO-L-3), 936.35/956.10 eV (GO-CuO-L-3) and 935.34/955.10 eV (rGO-CuO-L-3). These components were used to account for the complex multiplet structure of Cu(II) and were not interpreted as separate copper oxidation states. The characteristic shake-up satellite peak was located at approximately 942.40 eV (CuO-L-3), 943.41 eV (GO-CuO-L-3) and 942.46 eV (rGO-CuO-L-3), confirming that copper was predominantly present in the Cu(II) oxidation state. This assignment was further supported by the Cu LMM Auger spectra (Figure S1), which exhibited the characteristic Cu $L_3M_{45}M_{45}$ maximum at 917.5 eV in all investigated samples [64].

Compared with pristine CuO-L-3, the GO-CuO-L-3 composite exhibited a positive shift of the Cu $2p_{3/2}$ component from 933.52 to 934.56 eV, suggesting modification of the local chemical environment of surface Cu(II) species after incorporation of GO [65]. In contrast, the

Cu $2p_{3/2}$ binding energy of rGO-CuO-L-3 was 933.65 eV, close to that of pristine CuO-L-3, indicating a surface Cu(II) environment more similar to that of pristine CuO. Because differences in surface charging may also contribute to binding-energy shifts, this interpretation should be considered with appropriate caution [66].

The corresponding high-resolution O 1s spectra (Figure 3B, D and F) were dominated by the lattice oxygen peak (Cu–O), located at 529.78 eV (CuO-L-3, Figure 3B), 529.85 eV (GO-CuO-L-3, Figure 3D), and 529.87 eV (rGO-CuO-L-3, Figure 3F). A second component attributed to surface hydroxyl groups and other higher-binding-energy oxygen species was observed at 531.55, 531.17, and 531.65 eV, respectively. In the O 1s spectrum of GO-CuO-L-3 (Figure 3D), additional contributions centred at 533.14 and 535.20 eV were detected. The component at 533.14 eV was assigned to oxygen-containing surface functionalities associated with GO, including C–O and C–OH groups. The weak high-binding-energy component at 535.20 eV was attributed more conservatively to weakly adsorbed surface species rather than specifically to adsorbed H_2O. In rGO-CuO-L-3 (Figure 3F), the higher-binding-energy oxygen contributions were less pronounced than in GO-CuO-L-3, consistent with the lower abundance of oxygen-containing functional groups following GO reduction.

Overall, the XPS results confirmed that Cu(II) remained the predominant copper oxidation state in CuO, GO-CuO, and rGO-CuO. Incorporation of GO and rGO did not produce a distinct additional copper oxidation state but modified the local chemical environment of surface Cu(II) species and the abundance of oxygen-containing surface functionalities. These findings complement the XRD results by confirming that Cu(II) remained the predominant surface oxidation state after incorporation of GO and rGO.

Raman spectroscopy was employed to investigate the structural evolution in CuO NPs prepared at different calcination temperatures and interaction with GO and rGO. Prior to

quantitative analysis, all spectra were subjected to baseline correction to minimize the influence of fluorescence background. The Raman spectra of pure CuO samples (Figure 4A) exhibited the characteristic vibration modes of monoclinic CuO. The dominant band observed at approximately 280–290 cm^{-1} was assigned to the *Ag* mode, while broad bands located in the 320–350 cm^{-1} are assigned to *Bg* modes, consistent with the monoclinic crystal structure of CuO [67]. A weaker broad feature in the region of approximately 600–650 cm^{-1} was also observed, corresponding to an additional *Bg* mode of CuO. No pronounced Raman bands attributable to other crystalline copper oxide phases were detected, suggesting the absence of major secondary phases. Nevertheless, the relatively high fluorescence background and the limited sensitivity of Raman spectroscopy to minor phases mean that the presence of low amounts of secondary phases cannot be completely excluded based on Raman data alone. The position of the characteristic CuO Raman bands remained relatively consistent among the samples prepared at different calcination temperatures, with no pronounced systematic peak shifts being observed. This indicates that calcination did not substantially alter the CuO crystal phase. The changes in the spectral profiles, particularly in the definition and relative prominence of the characteristic CuO bands, are instead consistent with changes in structural ordering and crystallinity induced by calcination. These observations are in agreement with the XRD results, which indicate improved crystallinity at higher calcination. The Raman spectra of the GO-CuO-L-3 and rGO-CuO-L-3 nanocomposites (Figure 4B) exhibited the characteristic D and G bands associated with graphene-based carbon materials. For GO-CuO-L-3, the D and G bands were centred at approximately 1388 and 1598 cm^{-1}, respectively, resulting in an I_D/I_G ratio of 0.85. Following reduction to rGO, the D and G bands were observed at approximately 1347 and 1600 cm^{-1}, respectively, with a slightly increased I_D/I_G ratio of 0.89. The G band therefore remained at a comparable position, whereas the D band shifted towards lower wavenumbers after reduction. The modest increase in the I_D/I_G ratio is consistent with structural

458 rearrangement of the graphene framework during GO reduction, which can involve removal of
459 oxygen-containing functional groups accompanied by changes in the size and distribution of
460 sp^2 carbon domains. Similar increases in the I_D/I_G ratio following GO reduction have been
461 reported for related rGO-based copper nanocomposites [68].

462 **Inhibitory activity (*in vitro*)**

463 Figure 5 and Table S2 summarize the percentage inhibition of selected GTD pathogens by
464 newly synthesized CuO NPs. NPs without graphene oxide or reduced graphene oxide showed
465 markedly higher antifungal activity than graphene-modified formulations. While graphene-
466 containing NPs significantly inhibited two to four pathogens, CuO NPs without graphene
467 additives inhibited five of the tested species indicating a broader-spectrum antifungal activity
468 compared to graphene-modified formulations. The strongest inhibition was observed for CuO-
469 L-7 against *F. mediterranea* (69.05 %). In contrast, *D. seriata*, *Neonectria* sp., and *P. minimum*
470 showed high tolerance to CuO or graphene-modified NPs, with no significant inhibition
471 detected for any treatment. Similarly, *B. dothidea* exhibited significant inhibition only with
472 CuO-L-7 at 10× dilution (28.90 %), although all these pathogens were inhibited by the fungicide
473 Tessior (positive control). *E. lata* also displayed relatively high tolerance, with significant
474 inhibition detected only for undiluted rGO-CuO-L-3 (37.82 %), GO-CuO-L-1 (19.29 %), GO-
475 CuO-L-3 (25.07 %), and CuO-L-9 (42.26 %). In contrast, *F. mediterranea* was among the most
476 susceptible pathogens tested, with several Cu-based NP formulations causing significant
477 inhibition (19.79–69.05%, depending on NP formulation and dilution). However, the response
478 differed among formulations, and not all treatments were equally effective. In comparison, the
479 positive control Tessior resulted only in a non-significant reduction in mycelial growth.
480 *P. richardsiae* was significantly inhibited only by CuO NPs (CuO-L-3, CuO-L-7, and CuO-L-
481 9), with inhibition ranging from 22.32 % to 43.92 % depending on dilution. Similarly,
482 *F. oxysporum* showed greater sensitivity to CuO NPs without graphene additives. Significant

inhibition was observed for CuO-L-3, CuO-L-7, and CuO-L-9 (21.36–42.51 %), as well as for undiluted rGO-CuO-L-2 (19.55 %), GO-CuO-L-1 (26.57 %), GO-CuO-L-2 (29.54 %), and GO-CuO-L-3 at 10× dilution (19.71 %). A comparable trend was observed for *D. torresensis*, where significant inhibition was mainly associated with CuO-L-3, CuO-L-7, and CuO-L-9 (25.05–41.59 %), and with undiluted GO-CuO-L-3 (23.16 %). Based on these findings, CuO NPs without graphene derivatives were selected for further evaluation together with the pathogens *D. torresensis*, *F. oxysporum*, and *P. richardsiae* in the subsequent *in planta* experiment. Although *F. mediterranea* exhibited the highest *in vitro* sensitivity to CuO NPs, it was not included in the *in planta* experiment because its slow wood-colonizing lifestyle and cultivation characteristics make it less suitable for short-term assays. This selection was further supported by the estimated apparent EC_{50} values (Table S3), which were calculated only for treatments exhibiting a clear concentration-dependent response. Among these treatments, CuO NPs generally showed the lowest estimated EC_{50} values, ranging from 6.6 mg L^{-1} Cu (CuO-L-7 against *F. mediterranea*) to 8830.5 mg L^{-1} Cu (CuO-L-9 against *F. oxysporum*). However, these values should be interpreted with caution because they were derived from linear regression based on a limited number of tested concentrations and were estimated only for treatments with an approximately linear dose–response relationship.

Inhibitory activity (*in planta*)

As presented in Table 4 and Table S4, a statistically significant reduction in wood necrosis caused by *D. torresensis* was observed in plants treated with CuO-L-3 and CuO-L-9, corresponding to calculated inhibition values of 56.10 % and 21.22 %, respectively (Figure S2). Although CuO-L-7 resulted in a numerical inhibition of 29.61 %, the difference compared with the negative control was not statistically significant. No significant differences in grapevine height or root length were detected between any of the CuO treatments and the negative control for this pathogen.

In contrast, grapevines inoculated with *F. oxysporum* exhibited a significant increase in plant height in response to CuO-L-7 treatment, reaching 126.40±18.44 cm compared with 87.8±15.66 cm in the negative control. Neither CuO-L-3 nor CuO-L-9 significantly affected plant height. However, all three CuO treatments significantly increased root length, reaching 29.8±4.44 cm (CuO-L-3), 33.80±4.03 cm (CuO-L-7), and 28.20±4.87 cm (CuO-L-9), compared with 17.00±2.55 cm in the negative control. Significant reductions in wood necrosis were associated with CuO-L-7 and CuO-L-9, corresponding to calculated inhibition values of 47.67 % and 44.30 %, respectively. Although CuO-L-3 resulted in a numerical inhibition of 19.26 %, this reduction was not statistically significant (Figure S3).

For grapevines inoculated with *P. richardsiae*, none of the CuO treatments significantly affected root length compared with the negative control. Plant height was significantly increased only in plants treated with CuO-L-9, reaching 123.80±18.49 cm compared with 95.20±8.29 cm in the negative control. Although CuO-L-3 increased the mean plant height to 122.80±25.27 cm, this difference was not statistically significant. Regarding pathogen suppression, a significant reduction in wood necrosis was observed only following treatment with CuO-L-3, corresponding to a calculated inhibition value of 52.53 %. The reductions observed with CuO-L-7 (22.67 %) and CuO-L-9 (29.77 %) were not statistically significant (Figure S4).

Re-isolation and molecular identification of pathogens

The frequency of successful pathogen re-isolation is summarized in Table 5. The inoculated pathogens were consistently re-isolated from most inoculated grapevines, confirming successful colonization and infection of the host tissues. Across treatments, the target pathogens were recovered from 4 to 5 plants (80–100%). In addition to the inoculated fungi, occasional non-target fungal isolates were also recovered, most likely representing naturally occurring endophytic fungi or microorganisms associated with nursery-grown planting material.

Nevertheless, the successful re-isolation of the target pathogens provides strong evidence that the observed symptoms were associated with the experimental inoculations.

Gene expression profiling

Gene expression analysis revealed treatment- and pathogen-dependent variations in the expression of the target genes. Detailed results of the statistical analyses are provided in Table S5.

No significant effect was detected for VvPR1 under any treatment (Figure 6A). For VvNPR1, a statistically significant response was observed in two cases: in CuO-L-7–treated plants inoculated with *F. oxysporum* and in CuO-L-9–treated plants inoculated with *P. richardsiae*. However, only the latter exhibited a ≥2-fold increase in expression, indicating true upregulation, whereas the former did not reach this threshold despite being statistically significant (Figure 6B). The most pronounced responses were observed for VvSTS and VvChit4c. In plants inoculated with *D. torresensis*, VvSTS was consistently upregulated across all treatments, which was also supported by statistical analysis. In contrast, VvSTS was downregulated in plants inoculated with *F. oxysporum* and treated with CuO-L-7 and CuO-L-9. For *P. richardsiae*, significant upregulation of VvSTS was detected in CuO-L-3 and CuO-L-9 treatments, whereas CuO-L-7 induced only a moderate increase that did not exceed the 2-fold threshold and was not statistically significant (Figure 6C). For VvChit4c, statistically significant upregulation was observed in all treatments of plants inoculated with *D. torresensis*. In plants inoculated with *F. oxysporum*, VvChit4c was upregulated under CuO-L-3 treatment and downregulated under CuO-L-9. No significant changes in VvChit4c expression were detected in plants inoculated with *P. richardsiae* (Figure 6D).

To further resolve treatment specific transcriptional responses, OLS regression models were fitted separately for each pathogen using $\log_{10}$-transformed normalized gene expression values

(Figure 7). This analysis showed that CuO NPs induced distinct expression patterns depending on both pathogen identity and NP formulation. In plants inoculated with *D. torresensis* (Figure 7A–B), the strongest positive response was observed under CuO-L-3, particularly for VvChit4c, which showed the highest increase relative to the untreated control. A positive shift was also detected for VvSTS, whereas CuO-L-7 and CuO-L-9 produced weaker and less consistent responses across the analysed genes. In *F. oxysporum* inoculated plants (Figure 7C–D), the transcriptional response was more selective. CuO-L-3 was mainly associated with increased VvChit4c expression, while CuO-L-9 was associated with reduced VvSTS expression relative to the control. This contrast indicates that the tested CuO formulations differed not only in the magnitude but also in the direction of their effects on defence-related gene expression. In plants inoculated with *P. richardsiae*, the response pattern was more complex (Figure 7E–F). CuO-L-3 induced only moderate changes in gene expression, whereas CuO-L-9 was associated with increased expression of VvNPR1 and VvPR1, together with a positive shift in VvChit4c. Overall, the OLS models confirmed that CuO NPs did not trigger a uniform transcriptional response, but rather modulated grapevine defence gene expression in a pathogen and formulation dependent manner.

DISCUSSION

The morphological evolution observed by SEM well with structural changes revealed by the XRD results. Higher calcination temperatures produced CuO NPs with a more regular morphology, while the simultaneous narrowing and increased intensity of the diffraction peaks indicated improved crystallinity. Together, these observations demonstrate that calcination promoted structural ordering and crystal growth without altering the CuO crystal phase. The distinct sheet-like morphology of GO and the more folded structure of rGO were preserved after CuO deposition, indicating that incorporation of CuO did not disrupt the graphene-based supports. Together with the XPS results confirming the predominance of Cu(II), these

582 observations demonstrate the successful incorporation of CuO NPs into the GO and rGO based
583 supports without altering the CuO crystal phase.

584 The progressive narrowing and increasing intensity of the CuO diffraction peaks with
585 increasing calcination temperature indicate improved structural ordering and growth of the
586 coherent CuO crystallite domains. A similar temperature-dependent increase in CuO
587 crystallinity has been reported previously, with higher annealing temperatures producing more
588 intense peaks and reduced peak broadening [61,62]. The weak reflection at approximately 16°
589 observed in the pristine CuO samples may originate from a minor residual precursor-derived or
590 intermediate phase. However, its low intensity and the absence of additional characteristic
591 reflections do not allow an unambiguous phase assignment. Its decreasing intensity with
592 increasing calcination temperature nevertheless suggests progressive removal or transformation
593 of this minor phase during thermal treatment. The absence of distinct GO or rGO related
594 reflections may be attributed to their relatively low content, limited long-range ordering, and
595 the dominant diffraction intensity of crystalline CuO.

596 The XPS results confirmed that Cu(II) was the predominant oxidation state in all investigated
597 materials, as demonstrated by the characteristic Cu 2p shake-up satellite structure. The binding
598 energies observed for pristine CuO and rGO-CuO were consistent with those commonly
599 reported for CuO, whereas the shift of the main Cu $2p_{3/2}$ component to higher binding energy
600 in GO-CuO may be consistent with an interaction between surface Cu(II) species and the
601 oxygen-containing functional groups of GO [64]. Such interaction could modify the local
602 chemical environment of copper without changing its predominant oxidation state. The O 1s
603 spectra supported the presence of lattice oxygen associated with CuO in all samples [69]. In
604 GO-CuO, additional higher-binding-energy contributions were attributed to C–O and C–OH
605 functionalities originating from GO. The absence of a similarly pronounced contribution in
606 rGO-CuO is consistent with the lower abundance of oxygen-containing functional groups

607 expected after GO reduction. Overall, incorporation of GO and rGO preserved the CuO
608 chemical state but altered the surface environment of the NPs, which may influence their
609 interactions with biological systems.

610 Raman spectroscopy complemented the XRD and XPS results by confirming the
611 characteristic vibrational modes of monoclinic CuO and the presence of graphene-based
612 supports in the nanocomposites. The slightly higher I_D/I_G ratio observed for rGO-CuO than for
613 GO-CuO is consistent with structural rearrangement of the carbon framework during GO
614 reduction. A similar increase in the I_D/I_G after GO reduction was previously observed in a
615 related rGO-based copper nanocomposite [68].

616 The complementary physicochemical characterization confirmed the successful synthesis of
617 crystalline CuO NPs and GO-CuO/rGO-CuO nanocomposites. XRD, SEM and XPS
618 demonstrated that incorporation of graphene-based supports preserved the monoclinic CuO
619 phase and the Cu(II) oxidation state while primarily modifying the surface characteristics of the
620 nanocomposites.

621 The present study indicates that CuO NPs exhibit pathogen-dependent antifungal activity
622 under *in vitro* conditions, while selected formulations significantly reduced wood necrosis in
623 grapevines under controlled *in planta* conditions. Similar antifungal efficacy of CuO NPs has
624 been widely reported against a range of phytopathogenic fungi, including *A. alternata,*
625 *Alternaria mali* Roberts*, B. cinerea, D. seriata, F. oxysporum, Phomopsis vexans* (Sacc. &
626 P.Syd.) Harter, or *Ralstonia solanacearum* (Smith, 1896) Yabuuchi et al., 1996, confirming
627 their broad-spectrum antimicrobial potential [18,32,70–73]. Notably, CuO NPs without
628 graphene-based modifications generally exhibited higher antifungal activity than GO-CuO and
629 rGO-CuO nanocomposites, suggesting that the incorporation of graphene derivatives did not
630 improve antifungal efficacy under the tested conditions. This observation is supported by the

physicochemical characterization. XRD confirmed that incorporation of GO and rGO did not alter the monoclinic CuO crystal structure, while XPS demonstrated that Cu(II) remained the predominant oxidation state in all materials. SEM further demonstrated that CuO NPs remained distributed on both graphene-based supports, suggesting that the lower antifungal activity of GO-CuO and rGO-CuO was more likely associated with modification of the CuO surface environment than with a change in the CuO crystal phase or oxidation state. This may be explained by differences in NP surface reactivity and copper ion availability. The antifungal activity of CuO NPs is largely attributed to the release of Cu(II) ions and the generation of reactive oxygen species (ROS), which disrupt fungal cell membranes and metabolic processes [71,74,75]. The presence of graphene-based materials may partially modify the accessibility of the CuO surface and consequently influence NP-cell interactions and copper ion availability. An important limitation of this study is that the experimental design did not include a soluble copper treatment (e.g., $CuSO_4$) for comparison. Consequently, the respective contributions of NP-specific effects and copper ion release to the observed antifungal activity could not be separated. Nevertheless, the consistently higher efficacy of CuO NPs compared with GO-CuO and rGO-CuO formulations, despite their comparable copper content, suggests that NP physicochemical properties also play an important role in determining antifungal performance.

The antifungal activity observed in this study was strongly pathogen-dependent. While *F. mediterranea* exhibited high sensitivity, other pathogens such as *D. seriata* and *Neonectria* sp. showed considerable tolerance. Similar variability in microbial sensitivity to copper-based NPs has been widely reported, with susceptibility depending on organism-specific traits, NP properties, and experimental conditions [75]. This variability is commonly attributed to differences in fungal cell wall structure, detoxification mechanisms, and oxidative stress tolerance. However, the efficiency of these mechanisms depends on the ability of individual fungal species to mitigate oxidative stress or regulate intracellular metal homeostasis [76,77].

These findings highlight the importance of evaluating the efficacy of CuO NPs across a broad spectrum of pathogens before considering their practical use in grapevine protection strategies.

Importantly, the *in planta* results demonstrated that the antifungal potential observed under *in vitro* conditions was also reflected in reduced wood necrosis in grapevine plants, although the magnitude and statistical significance of these effects varied among pathogens and CuO NPs formulations. Comparable studies have shown that CuO NPs can significantly reduce disease severity under greenhouse and field conditions; for example, they have been reported to decrease necrosis and enhance growth parameters in cucumber plants infected with *F. oxysporum* [78]. Similar results have been reported for CuO NPs in chickpea, where they reduced *F. oxysporum* wilt severity and enhanced plant growth, likely through the activation of plant defence responses. Notably, lower concentrations were more effective, highlighting their dual role as antifungal agents and defense elicitors [79]. Preventive application of CuO NPs in grapevine has also been shown to reduce the incidence of fungal diseases associated with *A. alternata* and *A. niger*. Under curative conditions, these NPs were even able to halt disease progression in already infected plants. Importantly, no adverse effects on plant growth or flowering were observed, indicating the absence of phytotoxicity [48]. Collectively, these studies confirm that the antifungal activity of CuO NPs is not limited to artificial conditions but translates into biologically relevant outcomes in grapevine systems. Consistent with these observations, selected CuO NP treatments significantly reduced wood necrosis in grapevines inoculated with *D. torresensis*, *F. oxysporum*, and *P. richardsiae*. Improvements in growth parameters were most evident in plants inoculated with *F. oxysporum*, whereas responses varied among treatments and pathogens. Nevertheless, these results should be interpreted within the context of the experimental design. The *in planta* validation was performed under controlled conditions using only three GTD-associated pathogens, a single grapevine cultivar/rootstock combination (Sauvignon Blanc/SO4), and a single assessment conducted six months after

inoculation. Therefore, the present study should be considered a proof-of-concept demonstrating the biological potential of CuO NPs under controlled conditions rather than direct evidence of their efficacy in vineyard environments.

Beyond their direct antifungal activity, CuO NPs also modulated plant defence responses at the molecular level, with patterns that closely reflected pathogen-specific responses observed in this study. The upregulation of VvSTS in plants inoculated with *D. torresensis* and *P. richardsiae*, particularly under CuO-L-3 and CuO-L-9 treatments, suggests a potential stimulation of the stilbene biosynthetic pathway, which is involved in the production of phytoalexins such as resveratrol. Stilbenes represent key defence compounds in grapevine and play an important role in restricting fungal colonization in woody tissues [80–82]. In contrast, the downregulation of VvSTS observed in *F. oxysporum*–inoculated plants treated with CuO-L-7 and CuO-L-9 highlighting that NP-induced defence responses are highly context-dependent and shaped by both pathogen identity and nanomaterial properties. This interpretation is consistent with grapevine studies showing that VvSTS expression and stilbene accumulation are finely tuned according to the type of pathogen and environmental stimulus [83–85].

Similarly, the increased expression of VvChit4c across all treatments in *D. torresensis*–inoculated plants suggests a possible involvement of chitinase-mediated defence responses, which are known to contribute to fungal cell wall degradation and plant resistance [86,87]. In contrast, the variable expression of VvChit4c in *F. oxysporum*–infected plants, including downregulation under CuO-L-9 treatment, indicates a more complex interaction between the host, pathogen, and NP treatment. The absence of significant changes in VvChit4c expression in *P. richardsiae*–inoculated plants further highlights the pathogen-specific nature of these responses, as differential activation of chitinase genes depending on the infecting pathogen has been widely reported in plant–pathogen interactions [87,88]. Increasing evidence indicates that

metal-based NPs can activate plant defence pathways through ROS-mediated signalling, leading to transcriptional reprogramming and induction of defence-related genes [89–91].

The OLS based analysis further supported this interpretation by showing that CuO induced transcriptional responses were not uniform but depended on both pathogen identity and NP formulation. In *D. torresensis* inoculated plants, CuO-L-3 produced the strongest and most consistent positive shift, particularly in VvChit4c, together with increased VvSTS expression, suggesting a coordinated activation of chitinase mediated and stilbene associated defence responses. In *F. oxysporum* inoculated plants, the response was more selective, with CuO-L-3 mainly associated with VvChit4c induction, whereas CuO-L-9 was linked to reduced VvSTS expression. This indicates that different CuO formulations may redirect the balance between defence pathways rather than simply increasing overall defence gene expression. In *P. richardsiae* inoculated plants, CuO-L-9 was associated with positive shifts in VvNPR1 and VvPR1 expression, suggesting that systemic acquired resistance (SAR)-related signalling may contribute to the response in specific pathogen NP combinations.

Therefore, the absence of a broad significant response in VvPR1 and the limited activation of VvNPR1 in the ANOVA based evaluation suggest that salicylic acid dependent SAR was not uniformly induced across all treatments. However, the OLS based patterns indicate that SAR related markers may still be involved in specific interactions, particularly under CuO-L-9 treatment in *P. richardsiae* inoculated plants. Together, these findings suggest that CuO NPs do not activate a single conserved defence pathway but rather modulate the relative contribution of chitinase mediated defence, stilbene biosynthesis, and SAR associated signalling depending on the pathogen and NP formulation.

Overall, the combined physicochemical characterization and biological evaluation suggest that CuO NPs may influence grapevine–pathogen interactions through both antifungal activity

and modulation of host defence-related gene expression. The physicochemical analyses confirmed the successful synthesis of crystalline CuO NPs and demonstrated that the incorporation of GO and rGO modified their surface characteristics without improving antifungal efficacy under the tested conditions. Gene expression analysis revealed treatment- and pathogen-dependent changes in genes associated with stilbene biosynthesis, chitinase-mediated defence, and systemic acquired resistance. However, the underlying molecular mechanisms and their contribution to disease suppression remain to be elucidated. Together, these findings support further investigation of CuO NPs as potential tools for targeted GTD management.

Although CuO NPs represent a promising alternative to conventional copper-based fungicides, their long-term environmental safety requires careful consideration before practical implementation. The environmental fate and bioavailability of Cu-based NPs are influenced by several factors, including soil pH, organic matter content, mineral composition, and microbial activity, which collectively determine NP dissolution, transformation, and Cu^{2+} release [92,93]. Consequently, their behaviour under field conditions may differ substantially from that observed under controlled laboratory or nursery experiments. One of the major concerns associated with repeated application of Cu-based nanomaterials is the potential accumulation of copper in agricultural soils. Although NP formulations may enable lower application rates than conventional copper products, prolonged use could still result in increased copper concentrations, potentially affecting soil fertility and ecosystem functioning. Excessive copper exposure has been associated with phytotoxicity, impaired photosynthesis, oxidative stress, and disturbances in nutrient uptake in susceptible plant species [94,95]. Similarly, the antimicrobial properties responsible for pathogen suppression may also influence non-target soil microorganisms. Beneficial bacteria, fungi, and mycorrhizal communities play essential roles in nutrient cycling, soil structure, and plant health, and their long-term exposure to Cu-based

NPs may alter microbial diversity and ecosystem functions. However, recent studies indicate that these effects depend strongly on NP characteristics, soil properties, and exposure conditions, and may differ substantially from those caused by soluble copper salts. In some soils, CuO NPs exhibited considerably lower bioavailability and smaller impacts on microbial communities than $CuSO_4$, suggesting that NP behaviour cannot be directly inferred from dissolved copper toxicity alone [96–98]. No visible phytotoxic symptoms were reported in the treated grapevines, and improvements in selected growth parameters were observed in some treatment groups. Nevertheless, these observations do not exclude potential physiological effects or long-term phytotoxicity, which were not specifically assessed in the present study. Nevertheless, these findings should not be interpreted as evidence of long-term environmental safety. Additional studies evaluating NPs persistence, repeated applications, interactions with vineyard soils, effects on beneficial microbiota, and field-scale performance will be necessary before CuO NPs can be considered a sustainable alternative for GTD management.

CONCLUSION

From an applied perspective, the findings of this study are particularly relevant given the limited availability of effective control strategies against GTDs. Following the ban of sodium arsenite, alternative approaches are urgently needed. Cu-based NPs have been proposed as promising candidates for sustainable plant protection due to their potential antifungal activity and ability to modulate plant defence responses. However, several limitations should be considered. Although the present study provides promising results under controlled conditions, further research is required to evaluate long-term environmental impacts, NP persistence, and potential phytotoxicity. In addition, the effects of CuO NPs on non-target microorganisms and soil microbiota remain insufficiently understood.

In conclusion, this study provides novel evidence that selected CuO NP formulations can significantly reduce wood necrosis associated with GTD pathogens under controlled *in planta* conditions, while also modulating grapevine defence-related gene expression. Importantly, these effects were pathogen- and formulation-specific, indicating that CuO NPs do not induce a uniform transcriptional response but rather differentially affect the expression of host defence-related genes depending on the pathogen and NP variant. Pristine CuO NPs generally exhibited higher antifungal activity than GO-CuO and rGO-CuO nanocomposites, suggesting that incorporation of graphene-based supports did not improve their biological efficacy under the tested conditions. These findings highlight their potential as tools for targeted disease management in viticulture and provide a basis for future research on NP-based plant protection strategies. Future research should therefore focus on field-scale validation, long-term ecological impact assessment, and optimization of CuO NPs formulations for targeted GTD management.

ABBREVIATIONS

GTD(s) – grapevine trunk disease(s)

NP(s) – nanoparticle(s)

CuO NPs – copper oxide nanoparticles

GO-CuO NPs – copper oxide nanoparticles with graphene oxide

rGO-CuO NPs – copper oxide nanoparticles with reduced graphene oxide

BD – *Botryosphaeria dothidea*

DT – *Dactylonectria torresensis*

DS – *Diplodia seriata*

EL – *Eutypa lata*

FM – *Fomitiporia mediterranea*

FO – *Fusarium oxysporum*

Ne – *Neonectria* sp.

PM – *Phaeoacremonium minimum*

PR – *Pleurostoma richardsiae*

EC_{50} – half maximal effective concentration

ITS – internal transcribed spacer

VvACT – actin

VvPR1 – pathogenesis-related protein 1

VvNPR1 – non-expresser of pathogenesis-related gene 1

VvSTS – stilbene synthase

VvChit4c – acidic class IV chitinase

DECLARATIONS

Ethics approval and consent to participate

Not applicable.

Consent for publication

Not applicable.

Availability of data and material

All data generated or analysed during this study are included in this published article and its supplementary information files.

Funding

The work was supported from ERDF " Multidisciplinary research to increase application potential of nanomaterials in agricultural practice " (No. CZ.02.1.01/0.0/0.0/16_025/0007314). The authors also acknowledge the CzechNanoLab Research Infrastructure (ID 90251), supported by MEYS CR. The authors also like to acknowledge funding from CIISB, Instruct-CZ Centre, supported by MEYS CR grant numbers LM2023042 (CF Nanobiotechnology) and LUC24105. European Regional Development Fund-Project No. CZ.02.01.01/00/23_015/0008175. This outcome was also supported by the Ministry of Culture of the Czech Republic, from the NAKI III programme (ID: DH23P03OVV053).

Competing interests

The authors declare that they have no competing interests.

Acknowledgements

The authors gratefully acknowledge Zuzana Bytešníková for her supervision of the nanoparticle preparation.

Authors' contributions

A. Eichmeier, J. Čechová, and K. Štůsková designed the experimental framework. L. Richtera supervised the synthesis of the materials. J. Pekárková, E. Birgusová and A. Ridošková performed the physicochemical characterization and data interpretation of the synthesized nanomaterials. J. Pekárková contributed to drafting the sections of the manuscript related to

nanomaterial characterization. K. Štůsková conducted and evaluated the *in vitro* and *in planta* experiments and performed the statistical analyses. T. Kiss and K. Štůsková designed the gene expression analysis, performed real-time PCR, and evaluated treatment effects on grapevine gene expression profiles. L. Frejlichová performed the heatmap analysis of gene expression data. J. Čechová and K. Štůsková coordinated the preparation of the manuscript and drafted its main sections. A. Eichmeier supervised the study, approved the experimental design, and critically revised the manuscript.

Authors' information

[1]Mendeleum - Institute of Genetics, Faculty of Horticulture, Mendel University in Brno, 61300 Brno, Czech Republic

[2]Department of Chemistry and Biochemistry, Mendel University in Brno, 61300 Brno, Czech Republic

[3]Department of Microelectronics, Faculty of Electrical Engineering and Communication, Brno University of Technology, 616 00 Brno, Czech Republic

[4]Instituto de Ciencias de la Vid y del Vino (ICVV), Spanish National Research Council (CSIC), University of La Rioja and Government of La Rioja, 26007 Logroño, Spain

REFERENCES

1. Srilatha B. Nanotechnology in Agriculture. J Nanomedicine Nanotechnol. 2011; doi:10.4172/2157-7439.1000123.

2. Pestovsky YS, Martínez-Antonio A. The Use of Nanoparticles and Nanoformulations in Agriculture. J Nanosci Nanotechnol. 2017; doi:10.1166/jnn.2017.15041.

3. Savary S, Ficke A, Aubertot J-N, Hollier C. Crop losses due to diseases and their implications for global food production losses and food security. Food Secur. 2012; doi:10.1007/s12571-012-0200-5.

4. R4P Network. Trends and Challenges in Pesticide Resistance Detection. Trends Plant Sci. 2016; doi:10.1016/j.tplants.2016.06.006.

5. Miller SA, Ferreira JP, LeJeune JT. Antimicrobial Use and Resistance in Plant Agriculture: A One Health Perspective. Agriculture. 2022; doi:10.3390/agriculture12020289.

6. Islam T, Danishuddin, Tamanna NT, Matin MN, Barai HR, Haque MA. Resistance Mechanisms of Plant Pathogenic Fungi to Fungicide, Environmental Impacts of Fungicides, and Sustainable Solutions. Plants. 2024; doi:10.3390/plants13192737.

7. Prasad R, Bhattacharyya A, Nguyen QD. Nanotechnology in Sustainable Agriculture: Recent Developments, Challenges, and Perspectives. Front Microbiol. 2017; doi:10.3389/fmicb.2017.01014.

8. De Jong WH, Borm PJ. Drug delivery and nanoparticles: Applications and hazards. Int J Nanomedicine. Dove Medical Press. 2008; doi:10.2147/ijn.s596.

9. Kah M. Nanopesticides and Nanofertilizers: Emerging Contaminants or Opportunities for Risk Mitigation? Front Chem. 2015; doi:10.3389/fchem.2015.00064.

10. Peters RJB, Bouwmeester H, Gottardo S, Amenta V, Arena M, Brandhoff P, et al. Nanomaterials for products and application in agriculture, feed and food. Trends Food Sci Technol. 2016; doi:10.1016/j.tifs.2016.06.008.

881 11. Roy Choudhury S, Ghosh M, Mandal A, Chakravorty D, Pal M, Pradhan S, et al. Surface-
882 modified sulfur nanoparticles: an effective antifungal agent against *Aspergillus niger* and
883 *Fusarium oxysporum*. Appl Microbiol Biotechnol. 2011; doi:10.1007/s00253-011-3142-5.

884 12. Roy Choudhury S, Ghosh M, Goswami A. Inhibitory Effects of Sulfur Nanoparticles on
885 Membrane Lipids of A*spergillus niger*: A Novel Route of Fungistasis. Curr Microbiol. 2012;
886 doi:10.1007/s00284-012-0130-7.

887 13. Xu T, Hao W, Du R, Dai D, Wang C, Li S, et al. Mercaptoimidazole-capped gold
888 nanoparticles as a potent agent against plant pathogenic fungi. J Mater Chem B. Royal Society
889 of Chemistry. 2024; doi:10.1039/D4TB01032A.

890 14. Muhae-Ud-Din G, Abid R, Nazar S, Ghorbani A, Atta S, Chen M, et al. Antifungal
891 mechanisms and characterization of gold nanoparticles: a strategic approach to combat
892 *Colletotrichum capsici*-induced anthracnose disease and enhance chilli growth. Phytopathol
893 Res. 2025; doi:10.1186/s42483-025-00375-9.

894 15. Santhoshkumar T, Rahuman AA, Bagavan A, Marimuthu S, Jayaseelan C, Kirthi AV, et al.
895 Evaluation of stem aqueous extract and synthesized silver nanoparticles using *Cissus*
896 *quadrangularis* against *Hippobosca maculata* and *Rhipicephalus* (*Boophilus*) *microplus*. Exp
897 Parasitol. 2012; doi:10.1016/j.exppara.2012.06.009.

898 16. Mohamed NH, Ismail MA, Abdel-Mageed WM, Mohamed Shoreit AA. Antimicrobial
899 activity of latex silver nanoparticles using *Calotropis procera*. Asian Pac J Trop Biomed. 2014;
900 doi:10.12980/APJTB.4.201414B216.

901 17. Fernández JG, Fernández-Baldo MA, Berni E, Camí G, Durán N, Raba J, et al. Production
902 of silver nanoparticles using yeasts and evaluation of their antifungal activity against
903 phytopathogenic fungi. Process Biochem. 2016; doi:10.1016/j.procbio.2016.05.021.

18. Malandrakis AA, Kavroulakis N, Chrysikopoulos CV. Use of copper, silver and zinc nanoparticles against foliar and soil-borne plant pathogens. Sci Total Environ. 2019; doi:10.1016/j.scitotenv.2019.03.210.

19. Vizitiu DE, Sardarescu DI, Fierascu I, Fierascu RC, Soare LC, Ungureanu C, et al. Grapevine Plants Management Using Natural Extracts and Phytosynthesized Silver Nanoparticles. Materials. 2022; doi:10.3390/ma15228188.

20. Farahat G, Sehsahb MD, Salama NHH. Biosynthesis of Silver, Zinc, Titanium Nanoparticles Using Pathogenic Fungi: An Overview on Plant Disease supress, Toxicity and Safety. Environ Biodivers Soil Secur. 2023; doi:10.21608/jenvbs.2023.197433.1211.

21. Baroi AM, Fierascu I, Ghizdareanu A-I, Trica B, Fistos T, Matei (Brazdis) RI, et al. Green Approach for Synthesis of Silver Nanoparticles with Antimicrobial and Antioxidant Properties from Grapevine Waste Extracts. Int J Mol Sci. 2024; doi:10.3390/ijms25084212.

22. Ahmed A. Applications of Nickel Nanoparticles for Control of Fusarium Wilt on Lettuce and Tomato. Int J Innov Res Sci Eng Technol. 2016; doi:10.15680/IJIRSET.2016.0505132.

23. Parthasarathy R, Jayabaskaran C, Manikandan A, Anusuya S. Synthesis of Nickel-Chitosan Nanoparticles for Controlling Blast Diseases in Asian Rice. Appl Biochem Biotechnol. 2023; doi:10.1007/s12010-022-04198-8.

24. Abdallah Y, Ogunyemi SO, Bi J, Wang F, Huang X, Shi X, et al. Nickel oxide nanoparticles: A new generation nanoparticles to combat bacteria *Xanthomonas oryzae* pv. *oryzae* and enhance rice plant growth. Pestic Biochem Physiol. 2024; doi:10.1016/j.pestbp.2024.105807.

25. Velmurugan P, Shim J, Kim K, Oh B-T. *Prunus* × *yedoensis* tree gum mediated synthesis of platinum nanoparticles with antifungal activity against phytopathogens. Mater Lett. 2016; doi:10.1016/j.matlet.2016.03.069.

927 26. Kumar D, Soundhararajan R, Srinivasan H. Screening the efficacy of platinum-based
928 nanomaterial synthesized from *Allium sativum* to control plant pathogens. J Mater Sci Mater
929 Eng. 2024; doi:10.1186/s40712-024-00165-9.

930 27. Siddiqui ZA, Khan A, Khan MR, Abd-Allah EF. Effects of zinc oxide nanoparticles (ZnO
931 NPs) and some plant pathogens on the growth and nodulation of lentil (*Lens culinaris* Medik.).
932 Acta Phytopathol Entomol Hung. Akadémiai Kiadó. 2018; doi:10.1556/038.53.2018.012.

933 28. Siddiqui ZA, Parveen A, Ahmad L, Hashem A. Effects of graphene oxide and zinc oxide
934 nanoparticles on growth, chlorophyll, carotenoids, proline contents and diseases of carrot. Sci
935 Hortic. 2019; doi:10.1016/j.scienta.2019.01.054.

936 29. El-Abeid SE, Ahmed Y, Daròs J-A, Mohamed MA. Reduced Graphene Oxide Nanosheet-
937 Decorated Copper Oxide Nanoparticles: A Potent Antifungal Nanocomposite against Fusarium
938 Root Rot and Wilt Diseases of Tomato and Pepper Plants. Nanomaterials. 2020;
939 doi:10.3390/nano10051001.

940 30. Kalagatur NK, Nirmal Ghosh OS, Sundararaj N, Mudili V. Antifungal Activity of Chitosan
941 Nanoparticles Encapsulated With Cymbopogon martinii Essential Oil on Plant Pathogenic
942 Fungi *Fusarium graminearum*. Front Pharmacol. 2018; doi:10.3389/fphar.2018.00610.

943 31. Nandhini R, Rajeswari E, Harish S, Sivakumar V, Gangai Selvi R, Jaya sundrasharmila D.
944 Role of chitosan nanoparticles in sustainable plant disease management. J Nanoparticle Res.
945 2025; doi:10.1007/s11051-024-06203-z.

946 32. Banik S, Pérez-de-Luque A. *In vitro* effects of copper nanoparticles on plant pathogens,
947 beneficial microbes and crop plants. Span J Agric Res. 2017; doi:10.5424/sjar/2017152-10305.

948 33. Pariona N, I. Mtz-Enriquez A, Sánchez-Rangel D, Carrión G, Paraguay-Delgado F, Rosas-
949 Saito G. Green-synthesized copper nanoparticles as a potential antifungal against plant
950 pathogens. RSC Adv. Royal Society of Chemistry. 2019; doi:10.1039/C9RA03110C.

951 34. FAOSTAT. FAO Food Agric. Organ. U. N. Retrieved. 2024.
952 https://www.fao.org/faostat/en/#data/QCL. Accessed 2 Mar 2026.

953 35. Jordão AM, Correia AC. Grapevine Diversity and New Challenges in Grape Production.
954 IntechOpen. 2026; doi:10.5772/intechopen.1012190.

955 36. Mondello V, Songy A, Battiston E, Pinto C, Coppin C, Trotel-Aziz P, et al. Grapevine
956 Trunk Diseases: A Review of Fifteen Years of Trials for Their Control with Chemicals and
957 Biocontrol Agents. Plant Dis. 2018; doi:10.1094/PDIS-08-17-1181-FE.

958 37. Mugnai L, Graniti A, Surico G. Esca (Black Measles) and Brown Wood-Streaking: Two
959 Old and Elusive Diseases of Grapevines. Plant Dis. 1999; doi:10.1094/PDIS.1999.83.5.404.

960 38. Gramaje D, Úrbez-Torres JR, Sosnowski MR. Managing Grapevine Trunk Diseases With
961 Respect to Etiology and Epidemiology: Current Strategies and Future Prospects. Plant Dis.
962 2018; doi:10.1094/PDIS-04-17-0512-FE.

963 39. Claverie M, Notaro M, Fontaine F, Wery J. Current knowledge on Grapevine Trunk
964 Diseases with complex etiology: a systemic approach. Phytopathol Mediterr. 2020;
965 doi:10.36253/phyto-11150.

966 40. Bertsch C, Ramírez-Suero M, Magnin-Robert M, Larignon P, Chong J, Abou-Mansour E,
967 et al. Grapevine trunk diseases: complex and still poorly understood. Plant Pathol. 2013;
968 doi:10.1111/j.1365-3059.2012.02674.x.

969 41. Guerin-Dubrana L, Fontaine F, Mugnai L. Grapevine trunk disease in European and
970 Mediterranean vineyards: occurrence, distribution and associated disease-affecting cultural
971 factors. Phytopathol Mediterr. 2019; doi:10.14601/Phytopathol_Mediterr-25153.

972 42. Fontaine F, Gramaje D, Armengol J, Smart R, Nagy Z, Borgo M, et al. Grapevine Trunk
973 Diseases. A review. Paris, France: OIV Publications; 2016.

974 43. Pertot I, Prodorutti D, Colombini A, Pasini L. *Trichoderma atroviride* SC1 prevents
975 *Phaeomoniella chlamydospora* and *Phaeoacremonium aleophilum* infection of grapevine
976 plants during the grafting process in nurseries. BioControl. 2016; doi:10.1007/s10526-016-
977 9723-6.

978 44. Leal C, Gramaje D, Fontaine F, Richet N, Trotel-Aziz P, Armengol J. Evaluation of *Bacillus*
979 *subtilis* PTA -271 and *Trichoderma atroviride* SC1 to control Botryosphaeria dieback and
980 black-foot pathogens in grapevine propagation material. Pest Manag Sci. 2023;
981 doi:10.1002/ps.7339.

982 45. Eichmeier A, Pečenka J, Peňázová E, Baránek M, Català-García S, León M, et al. High-
983 throughput amplicon sequencing-based analysis of active fungal communities inhabiting
984 grapevine after hot-water treatments reveals unexpectedly high fungal diversity. Fungal Ecol.
985 2018; doi:10.1016/j.funeco.2018.07.011.

986 46. Štůsková K, Pečenka J, Tekielska DA, Špetík M, Bytešníková Z, Švec P, et al. The *in vitro*
987 effects of selected substances and nanomaterials against *Diaporthe eres*, *Diplodia seriata* and
988 *Eutypa lata*. Ann Appl Biol. 2022; doi:10.1111/aab.12812.

989 47. Štůsková K, Kiss T, Bytešníková Z, Richtera L, Gramaje D, Eichmeier A. Silver-selenium
990 nanoparticles and selected chemical compounds significantly inhibit grapevine trunk disease
991 pathogens. Pest Manag Sci. 2025; doi:10.1002/ps.70110.

992 48. Martínez-Soto D, Campos-Jiménez E, Cabello-Pasini A, Garcia-Marin LE, Meza-Villezcas
993 A, Castro-Longoria E. Evaluation of Fungal Sensitivity to Biosynthesized Copper-Oxide
994 Nanoparticles (CuONPs) in Grapevine Tissues and Fruits. J Fungi. 2025;
995 doi:10.3390/jof11100719.

996 49. Bytešníková Z, Koláčková M, Dobešová M, Švec P, Ridošková A, Pekárková J, et al. New
997 insight into the biocompatibility/toxicity of graphene oxides and their reduced forms on
998 *Chlamydomonas reinhardtii*. NanoImpact. 2023; doi:10.1016/j.impact.2023.100468.

999 50. Chauhan KR, Le TC, Chintakunta PK, Lakshman DK. Phyto-Fungicides: Structure Activity
1000 Relationships of the Thymol Derivatives against *Rhizoctonia solani*. J Agric Chem Environ.
1001 Scientific Research Publishing. 2017; doi:10.4236/jacen.2017.64012.

1002 51. Metsalu T, Vilo J. ClustVis: a web tool for visualizing clustering of multivariate data using
1003 Principal Component Analysis and heatmap. Nucleic Acids Res. 2015;
1004 doi:10.1093/nar/gkv468.

1005 52. Chacón-Vozmediano JL, Gramaje D, León M, Armengol J, Moral J, Izquierdo-Cañas PM,
1006 et al. Cultivar Susceptibility to Natural Infections Caused by Fungal Grapevine Trunk
1007 Pathogens in La Mancha Designation of Origin (Spain). Plants. 2021;
1008 doi:10.3390/plants10061171.

1009 53. White TJ, Bruns T, Lee S, Taylor J. Amplification and direct sequencing of fungal
1010 ribosomal RNA genes for phylogenetics. In PCR protocols a guide to methods and applications.
1011 PCR Protoc. 1990; doi:10.1016/B978-0-12-372180-8.50042-1.

1012 54. Altschul SF, Gish W, Miller W, Myers EW, Lipman DJ. Basic local alignment search tool.
1013 J Mol Biol. 1990; doi:10.1016/S0022-2836(05)80360-2.

1014 55. Le Henanff G, Heitz T, Mestre P, Mutterer J, Walter B, Chong J. Characterization of *Vitis*
1015 *vinifera* NPR1 homologs involved in the regulation of pathogenesis-related gene expression.
1016 BMC Plant Biol. 2009; doi:10.1186/1471-2229-9-54.

1017 56. Ramírez-Suero M, Bénard-Gellon M, Chong J, Laloue H, Stempien E, Abou-Mansour E,
1018 et al. Extracellular compounds produced by fungi associated with Botryosphaeria dieback
1019 induce differential defence gene expression patterns and necrosis in *Vitis vinifera* cv.
1020 Chardonnay cells. Protoplasma. 2014; doi:10.1007/s00709-014-0643-y.

1021 57. Eichmeier A, Baránek M, Pidra M. Analysis of genetic diversity and phylogeny of partial
1022 coat protein domain in Czech and Italian GFLV isolates. Plant Prot Sci. 2010;
1023 doi:10.17221/10/2010-PPS.

1024 58. Pfaffl MW. A new mathematical model for relative quantification in real-time RT–PCR.
1025 Nucleic Acids Res. 2001; doi:10.1093/nar/29.9.e45.

1026 59. Colin Cameron A, Miller DL. A Practitioner's Guide to Cluster-Robust Inference. J Hum
1027 Resour. 2015; doi:10.3368/jhr.50.2.317.

1028 60. Jońca J, Ryzhikov A, Palussière S, Esvan J, Fajerwerg K, Menini P, et al. Organometallic
1029 Synthesis of CuO Nanoparticles: Application in Low-Temperature CO Detection.
1030 ChemPhysChem. 2017; doi:10.1002/cphc.201700693.

1031 61. Vidyasagar CC, Arthoba Naik Y, Venkatesha TG, Viswanatha R. Solid-State Synthesis and
1032 Effect of Temperature on Optical Properties of CuO Nanoparticles. Nano-Micro Lett. 2012;
1033 doi:10.1007/BF03353695.

1034 62. Chan YB, Selvanathan V, Tey L-H, Akhtaruzzaman M, Anur FH, Djearamane S, et al.
1035 Effect of Calcination Temperature on Structural, Morphological and Optical Properties of

1036 Copper Oxide Nanostructures Derived from *Garcinia mangostana* L. Leaf Extract.
1037 Nanomaterials. Basel, Switzerland. 2022; doi:10.3390/nano12203589.

1038 63. Banu KB. Integrated experimental and DFT study of a GO–CuO nanocomposite with
1039 improved antifungal efficacy and photocatalytic behavior. Discov Chem. 2026;
1040 doi:10.1007/s44371-026-00595-8.

1041 64. Biesinger MC. Advanced analysis of copper X-ray photoelectron spectra. Surf Interface
1042 Anal. 2017; doi:10.1002/sia.6239.

1043 65. Zhang K, Suh JM, Lee TH, Cha JH, Choi J-W, Jang HW, et al. Copper oxide–graphene
1044 oxide nanocomposite: efficient catalyst for hydrogenation of nitroaromatics in water. Nano
1045 Converg. 2019; doi:10.1186/s40580-019-0176-3.

1046 66. Choi J, Oh H, Han S-W, Ahn S, Noh J, Park JB. Preparation and characterization of
1047 graphene oxide supported Cu, Cu2O, and CuO nanocomposites and their high photocatalytic
1048 activity for organic dye molecule. Curr Appl Phys. 2017; doi:10.1016/j.cap.2016.11.020.

1049 67. Cortés-Santiago A, Vicencio Garrido MA, Pacio M, Juárez Santiesteban H, Caballero-
1050 Briones F, Lozano-Espinosa M. Validation of the Cançado crystallite size model in rGO–
1051 CuO/Cu_2O nanocomposites: Raman-based statistical assessment. Appl Surf Sci. 2026;
1052 doi:10.1016/j.apsusc.2026.166568.

1053 68. Bytešníková Z, Pečenka J, Tekielska D, Kiss T, Švec P, Ridošková A, et al. Reduced
1054 graphene oxide-based nanometal-composite containing copper and silver nanoparticles protect
1055 tomato and pepper against *Xanthomonas euvesicatoria* infection. Chem Biol Technol Agric.
1056 2022; doi:10.1186/s40538-022-00347-7.

1057 69. Shultz LR, Preradovic K, Ghimire S, Hadley HM, Xie S, Kashyap V, et al. Nickel foam
1058 supported porous copper oxide catalysts with noble metal-like activity for aqueous phase
1059 reactions. Catal Sci Technol. 2022; doi:10.1039/D1CY02313F.

1060 70. Ahmad H, Venugopal K, Bhat AH, Kavitha K, Ramanan A, Rajagopal K, et al. Enhanced
1061 Biosynthesis Synthesis of Copper Oxide Nanoparticles (CuO-NPs) for their Antifungal Activity
1062 Toxicity against Major Phyto-Pathogens of Apple Orchards. Pharm Res. 2020;
1063 doi:10.1007/s11095-020-02966-x.

1064 71. Ashraf H, Anjum T, Riaz S, S. Ahmad I, Irudayaraj J, Javed S, et al. Inhibition mechanism
1065 of green-synthesized copper oxide nanoparticles from *Cassia fistula* towards *Fusarium*
1066 *oxysporum* by boosting growth and defense response in tomatoes. Environ Sci Nano. Royal
1067 Society of Chemistry. 2021; doi:10.1039/D0EN01281E.

1068 72. Khan M, Khan AA, Parveen A, Min K, Yadav VK, Khan AU, et al. Mitigating the growth
1069 of plant pathogenic bacterium, fungi, and nematode by using plant-mediated synthesis of copper
1070 oxide nanoparticles (CuO NPs). Green Chem Lett Rev. 2023;
1071 doi:10.1080/17518253.2023.2177520.

1072 73. Rabea A, Naeem E, Balabel NM, Daigham GE. Management of potato brown rot disease
1073 using chemically synthesized CuO-NPs and MgO-NPs. Bot Stud. 2023; doi:10.1186/s40529-
1074 023-00393-w.

1075 74. Meghana S, Kabra P, Chakraborty S, Padmavathy N. Understanding the pathway of
1076 antibacterial activity of copper oxide nanoparticles. RSC Adv. Royal Society of Chemistry.
1077 2015; doi:10.1039/C4RA12163E.

1078 75. Gudkov SV, Burmistrov DE, Fomina PA, Validov SZ, Kozlov VA. Antibacterial Properties
1079 of Copper Oxide Nanoparticles (Review). Int J Mol Sci. 2024; doi:10.3390/ijms252111563.

76. Zhang Z, Chen Y, Li B, Chen T, Tian S. Reactive oxygen species: A generalist in regulating development and pathogenicity of phytopathogenic fungi. Comput Struct Biotechnol J. 2020; doi:10.1016/j.csbj.2020.10.024.

77. Murugesan S, Balasubramanian S, Perumal E. Copper oxide nanoparticles induced reactive oxygen species generation: A systematic review and meta-analysis. Chem Biol Interact. 2025; doi:10.1016/j.cbi.2024.111311.

78. Kamel SM, Elgobashy SF, Omara RI, Derbalah AS, Abdelfatah M, El-Shaer A, et al. Antifungal Activity of Copper Oxide Nanoparticles against Root Rot Disease in Cucumber. J Fungi. 2022; doi:10.3390/jof8090911.

79. Tiwari V, Bambharoliya KS, Bhatt MD, Nath M, Arora S, Dobriyal AK, et al. Application of Green Synthesized Copper Oxide Nanoparticles for Effective Mitigation of Fusarium Wilt Disease in Roots of *Cicer Arietinum*. Rochester, NY: Social Science Research Network. 2023; doi:10.2139/ssrn.4566689.

80. Chong J, Poutaraud A, Hugueney P. Metabolism and roles of stilbenes in plants. Plant Sci. 2009; doi:10.1016/j.plantsci.2009.05.012.

81. Almagro L, Carbonell-Bejerano P, Belchí-Navarro S, Bru R, Martínez-Zapater JM, Lijavetzky D, et al. Dissecting the Transcriptional Response to Elicitors in *Vitis vinifera* Cells. PLOS ONE. 2014; doi:10.1371/journal.pone.0109777.

82. Huang L, Zhang S, Singer SD, Yin X, Yang J, Wang Y, et al. Expression of the Grape VqSTS21 Gene in Arabidopsis Confers Resistance to Osmotic Stress and Biotrophic Pathogens but Not *Botrytis cinerea*. Front Plant Sci. 2016; doi:10.3389/fpls.2016.01379.

1101 83. Gil-Muñoz R, Fernández-Fernández JI, Crespo-Villegas O, Garde-Cerdán T. Elicitors used
1102 as a tool to increase stilbenes in grapes and wines. Food Res Int. 2017;
1103 doi:10.1016/j.foodres.2016.11.035.

1104 84. Németh G, Hegyi O, Dunai A, Kocsis L. Stilbenes in the different organs of *Vitis vinifera*
1105 cv. Merlot grafted on Teleki Kober 5BB rootstock. OENO One. 2017; doi:10.20870/oeno-
1106 one.2016.50.4.1068.

1107 85. Pavela R, Waffo-Téguo P, Biais B, Richard T, Merillon J-M. *Vitis vinifera* canes, a source
1108 of stilbenoids against *Spodoptera littoralis* larvae. J Pest Sci. 2017; doi:10.1007/s10340-017-
1109 0836-1.

1110 86. Passarinho PA, de Vries SC. Arabidopsis Chitinases: a Genomic Survey. Arab Book. 2002;
1111 doi:10.1199/tab.0023.

1112 87. Grover A. Plant Chitinases: Genetic Diversity and Physiological Roles. Crit Rev Plant Sci.
1113 Taylor & Francis. 2012; doi:10.1080/07352689.2011.616043.

1114 88. El Hadrami A, Adam LR, El Hadrami I, Daayf F. Chitosan in Plant Protection. Mar Drugs.
1115 2010; doi:10.3390/md8040968.

1116 89. Rico CM, Majumdar S, Duarte-Gardea M, Peralta-Videa JR, Gardea-Torresdey JL.
1117 Interaction of Nanoparticles with Edible Plants and Their Possible Implications in the Food
1118 Chain. J Agric Food Chem. American Chemical Society. 2011; doi:10.1021/jf104517j.

1119 90. Dimkpa CO, Singh U, Bindraban PS, Adisa IO, Elmer WH, Gardea-Torresdey JL, et al.
1120 Addition-omission of zinc, copper, and boron nano and bulk oxide particles demonstrate
1121 element and size -specific response of soybean to micronutrients exposure. Sci Total Environ.
1122 2019; doi:10.1016/j.scitotenv.2019.02.142.

1123 91. Zulfiqar F, Navarro M, Ashraf M, Akram NA, Munné-Bosch S. Nanofertilizer use for
1124 sustainable agriculture: Advantages and limitations. Plant Sci Int J Exp Plant Biol. 2019;
1125 doi:10.1016/j.plantsci.2019.110270.

1126 92. Rajput V, Minkina T, Ahmed B, Sushkova S, Singh R, Soldatov M, et al. Interaction of
1127 Copper-Based Nanoparticles to Soil, Terrestrial, and Aquatic Systems: Critical Review of the
1128 State of the Science and Future Perspectives. Rev Environ Contam Toxicol. 2020;
1129 doi:10.1007/398_2019_34.

1130 93. Bakshi M, Kumar A. Copper-based nanoparticles in the soil-plant environment: Assessing
1131 their applications, interactions, fate and toxicity. Chemosphere. 2021;
1132 doi:10.1016/j.chemosphere.2021.130940.

1133 94. Kumar V, Pandita S, Singh Sidhu GP, Sharma A, Khanna K, Kaur P, et al. Copper
1134 bioavailability, uptake, toxicity and tolerance in plants: A comprehensive review.
1135 Chemosphere. 2021; doi:10.1016/j.chemosphere.2020.127810.

1136 95. Mir AR, Pichtel J, Hayat S. Copper: uptake, toxicity and tolerance in plants and
1137 management of Cu-contaminated soil. Biometals Int J Role Met Ions Biol Biochem Med. 2021;
1138 doi:10.1007/s10534-021-00306-z.

1139 96. Ameen F, Alsamhary K, Alabdullatif JA, ALNadhari S. A review on metal-based
1140 nanoparticles and their toxicity to beneficial soil bacteria and fungi. Ecotoxicol Environ Saf.
1141 2021; doi:10.1016/j.ecoenv.2021.112027.

1142 97. Rippner DA, Margenot AJ, Fakra SC, Aguilera LA, Li C, Sohng J, et al. Microbial response
1143 to copper oxide nanoparticles in soils is controlled by land use rather than copper fate. Environ
1144 Sci Nano. 2021; doi:10.1039/D1EN00656H.

1145 98. Samarajeewa AD, Velicogna JR, Schwertfeger DM, Princz JI, Subasinghe RM, Scroggins
1146 RP, et al. Ecotoxicological effects of copper oxide nanoparticles (nCuO) on the soil microbial
1147 community in a biosolids-amended soil. Sci Total Environ. 2021;
1148 doi:10.1016/j.scitotenv.2020.143037.

1149 99. Špetík M, Balík J, Híc P, Hakalová E, Štůsková K, Frejlichová L, et al. Lignans Extract
1150 from Knotwood of Norway Spruce—A Possible New Weapon against GTDs. J Fungi. 2022;
1151 doi:10.3390/jof8040357.

1152 100. Guarnaccia V, Groenewald JZ, Woodhall J, Armengol J, Cinelli T, Eichmeier A, et al.
1153 *Diaporthe* diversity and pathogenicity revealed from a broad survey of grapevine diseases in
1154 Europe. Persoonia - Mol Phylogeny Evol Fungi. 2018; doi:10.3767/persoonia.2018.40.06.

1155 101. Baránek M, Armengol J, Holleinová V, Pečenka J, Calzarano F, Peňázová E, et al.
1156 Incidence of symptoms and fungal pathogens associated with grapevine trunk diseases in Czech
1157 vineyards: first example from a north-eastern European grape-growing region. Phytopathol
1158 Mediterr. 2018; doi:10.14601/Phytopathol_Mediterr-22460.

1159 102. Crous PW, Osieck ER, Shivas RG, Tan YP, Bishop-Hurley SL, Esteve-Raventós F, et al.
1160 Fungal Planet description sheets: 1478–1549. Persoonia Mol Phylogeny Evol Fungi. 2023;
1161 doi:10.3767/persoonia.2023.50.05.

1162

TABLES

Table 1: Properties of the prepared nanomaterials and their stock suspensions used in the in vitro inhibitory assays against GTD pathogens. NA = not analysed due to incomplete digestion of the nanomaterial during Cu concentration determination. Concentration of nanomaterials in diluted solutions: 1× = 100 mg L^{-1}; 10 × = 10 mg L^{-1}; 100 × = 1 mg L^{-1}.

NPs	Calcination temperature [°C]	Cu content in the nanomaterial [mg g^{-1}]	Cu content in the stock solution [mg L^{-1}]	Dilutions applied in the *in vitro* experiment
rGO-CuO-L-1	300	844.22	84.42	1×, 10×, 100×
rGO-CuO-L-2	200	NA	NA	1×, 10×, 100×
rGO-CuO-L-3	400	805.21	80.52	1×, 10×, 100×
GO-CuO-L-1	300	893.58	89.36	1×, 10×, 100×
GO-CuO-L-2	200	766.49	76.65	1×, 10×, 100×
GO-CuO-L-3	400	972.40	97.24	1×, 10×, 100×
CuO-L-3	400	909.53	90.95	1×, 10×, 100×
CuO-L-7	200	831.38	83.14	1×, 10×, 100×
CuO-L-9	300	881.94	88.19	1×, 10×, 100×

Table 2: Description of fungal isolates associated with GTDs used in the in vitro inhibition assay of newly synthesized CuO NPs.

Pathogen	Name of isolate	Host plant	Accession number	Reference
Botryosphaeria dothidea	MEND-F-0196	Grapevine	-	unpublished
Dactylonectria torresensis	MEND-F-0016	Grapevine	-	Špetík *et al.*, 2022
Diaporthe ampelina	MEND-F-0766; CPC 29821	Grapevine	MG280996	Guarnaccia *et al.*, 2018
Diplodia seriata	MEND-F-0190	Grapevine	-	unpublished
Eutypa lata	MEND-F-0553; 13_3_4_KO	Grapevine	KY270968	Baránek *et al.*, 2018
Fomitiporia mediterranea	MEND-F-0473	Grapevine	-	unpublished
Fusarium oxysporum	MEND-F-0360	Grapevine	-	unpublished
Neonectria sp.	MEND-F-0788; CBS 145415	Prunus	OQ359119	Crous *et al.*, 2023
Phaeoacremonium minimum	MEND-F-0013	Grapevine	-	Špetík *et al.*, 2022
Pleurostoma richardsiae	MEND-F-0358	Grapevine	-	unpublished

Table 3: Primer sequences of selected genes used for qPCR analysis of grapevine seedlings treated with newly synthesized CuO NPs and inoculated with GTD pathogens. [a]GenBank accession number, [b]Genoscope Grape Genome Browser number.

Gene	Accession number	Forward Primer 5′ → 3′	Reverse Primer 3′ → 5′
VvACT	AF369524[a]	TGCTATCCTTCGTCTTGACCTTG	GGACTTCTGGACAACGGAATCTC
VvPR1	GSVIVT00038575001[b]	GGAGTCCATTAGCACTCCTTTG	CATAATTCTGGGCGTAGGCAG
VvNPR1	GSVIVT00016536001[b]	GGAATTCGATGTTGGGTACG	GCAACCTTGTCAAGAATGTCC
VvSTS	DQ366301[a]	CATCAAGGGTGCTATGCAGGT	TCAGAGCACACCACAAGAACTCG
VvChit4c	AY137377[a]	TCGAATGCGATGGTGGAAA	TCCCCTGTCGAAACACCAAG

Table 4: Effects of selected CuO nanoparticle treatments on grapevine height, root length, wood necrosis, and necrosis inhibition in plants inoculated with GTD pathogens under in planta conditions. Data are expressed as mean ± standard deviation (SD) from five biological replicates per treatment (n = 5), except for necrosis inhibition, which is expressed as a percentage relative to the negative control. DT – D. torresensis; FO – F. oxysporum; PR – P. richardsiae. Superscript [a] – indicates a statistically significant difference compared with the negative control (adjusted $p < 0.05$), as determined by the statistical procedures detailed in Table S4.

Pathogen	Parameter	CuO-L-3 10×	CuO-L-7 10×	CuO-L-9 10×	Negative control (tap water)
DT	Grapevine height (cm)	119.00±20.98	111.20±11.10	115.40±11.13	121.40±33.72
	Root length (cm)	25.40±5.81	31.80±6.22	25.60±4.45	26.20±5.59
	Necrosis (%)	36.37±26.26[a]	58.31±33.49	65.26±10.99[a]	82.84±5.89
	Inhibition (%)	56.10	29.61	21.22	0.00
FO	Grapevine height (cm)	95.20±13.08	126.40±18.44[a]	100.60±24.28	87.80±15.66
	Root length (cm)	29.80±4.44[a]	33.80±4.03[a]	28.20±4.87[a]	17.00±2.55
	Necrosis (%)	63.07±17.51	40.88±15.15[a]	43.51±26.26[a]	78.11±5.57
	Inhibition (%)	19.26	47.67	44.30	0.00
PR	Grapevine height (cm)	122.80±25.27	114.00±11.77	123.80±18.49[a]	95.20±8.29
	Root length (cm)	29.20±5.12	31.40±3.29	30.60±4.22	27.20±6.14
	Necrosis (%)	40.82±22.80[a]	66.50±34.43	60.40±20.40	85.99±7.02
	Inhibition (%)	52.53	22.67	29.77	0.00

Table 5: Re-isolation frequency of GTD pathogens from grapevine plants treated with CuO NPs. DT – D. torresensis, FO – F. oxysporum, PR – P. richardsiae.

		Number of plants		
Treatment	**Applied pathogen**	***Dactylonectria***	***Fusarium***	***Pleurostoma***
CuO-L-3	DT	4	2	0
	FO	0	4	0
	PR	0	0	4
CuO-L-7	DT	4	0	1
	FO	0	5	0
	PR	0	0	4
CuO-L-9	DT	5	0	1
	FO	0	4	0
	PR	1	0	5
Control (tap water)	DT	5	0	0
	FO	1	5	0
	PR	0	0	5

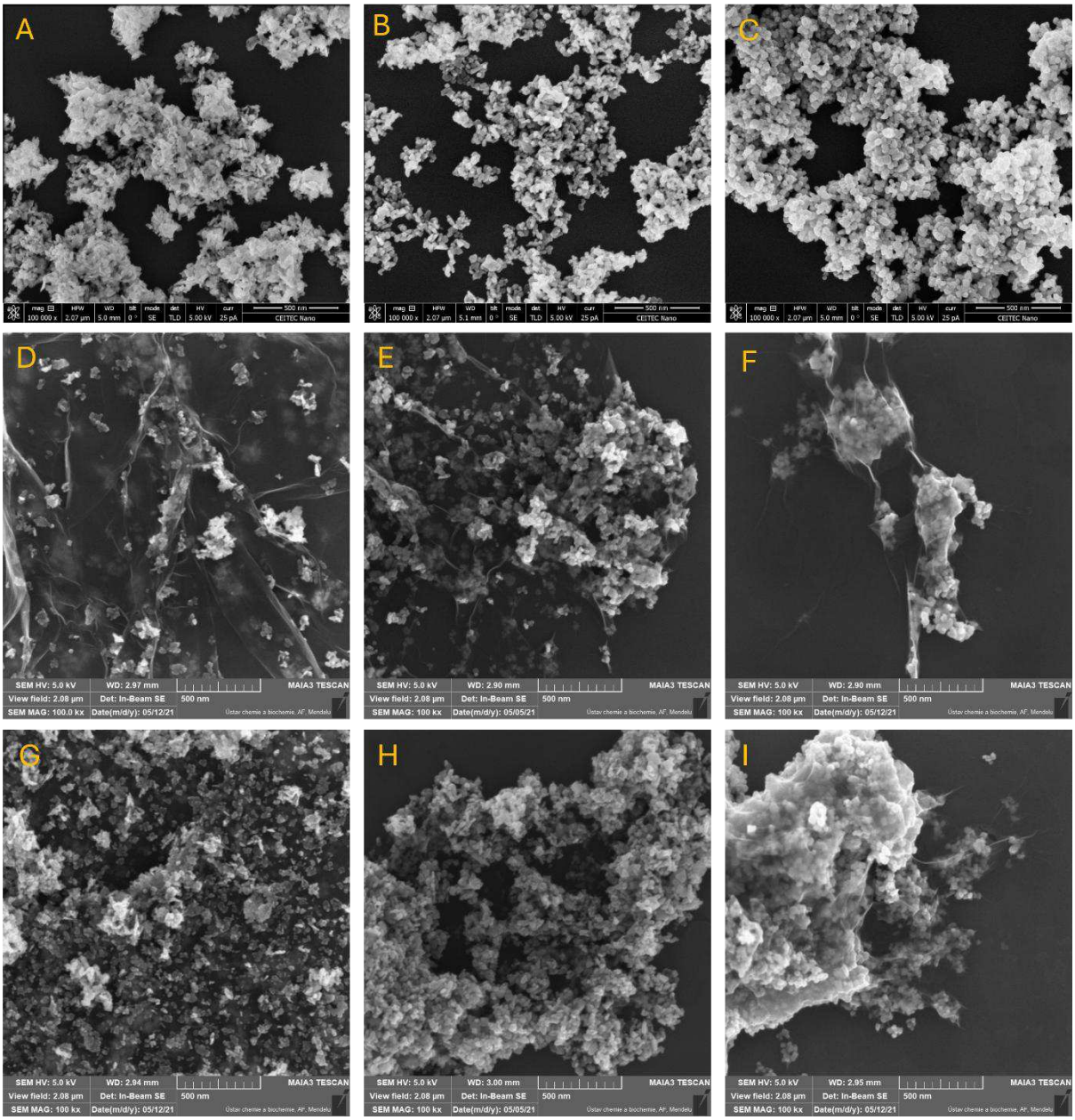

Figure 1: SEM images of pristine CuO (A–C), GO-CuO (D–F), and rGO-CuO (G–I) nanocomposites calcined at 200 °C (A, D, G), 300 °C (B, E, H), and 400 °C (C, F, I).

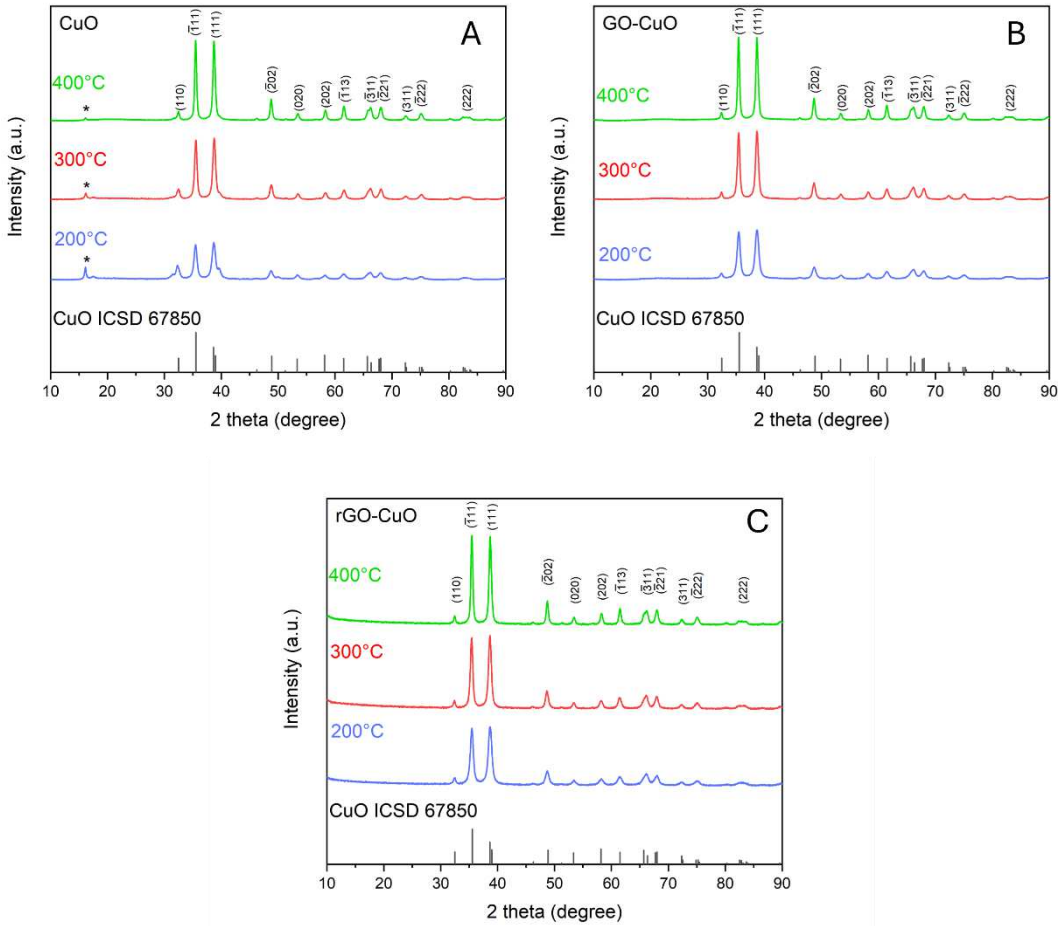

1192

1193 *Figure 2: X-ray diffraction (XRD) patterns of pristine CuO (A), GO-CuO (B), and rGO-CuO*
1194 *(C) nanocomposites calcined at 200, 300, and 400 °C. The asterisk (*) indicates a weak*
1195 *diffraction peak detected in pristine CuO samples.*

1196

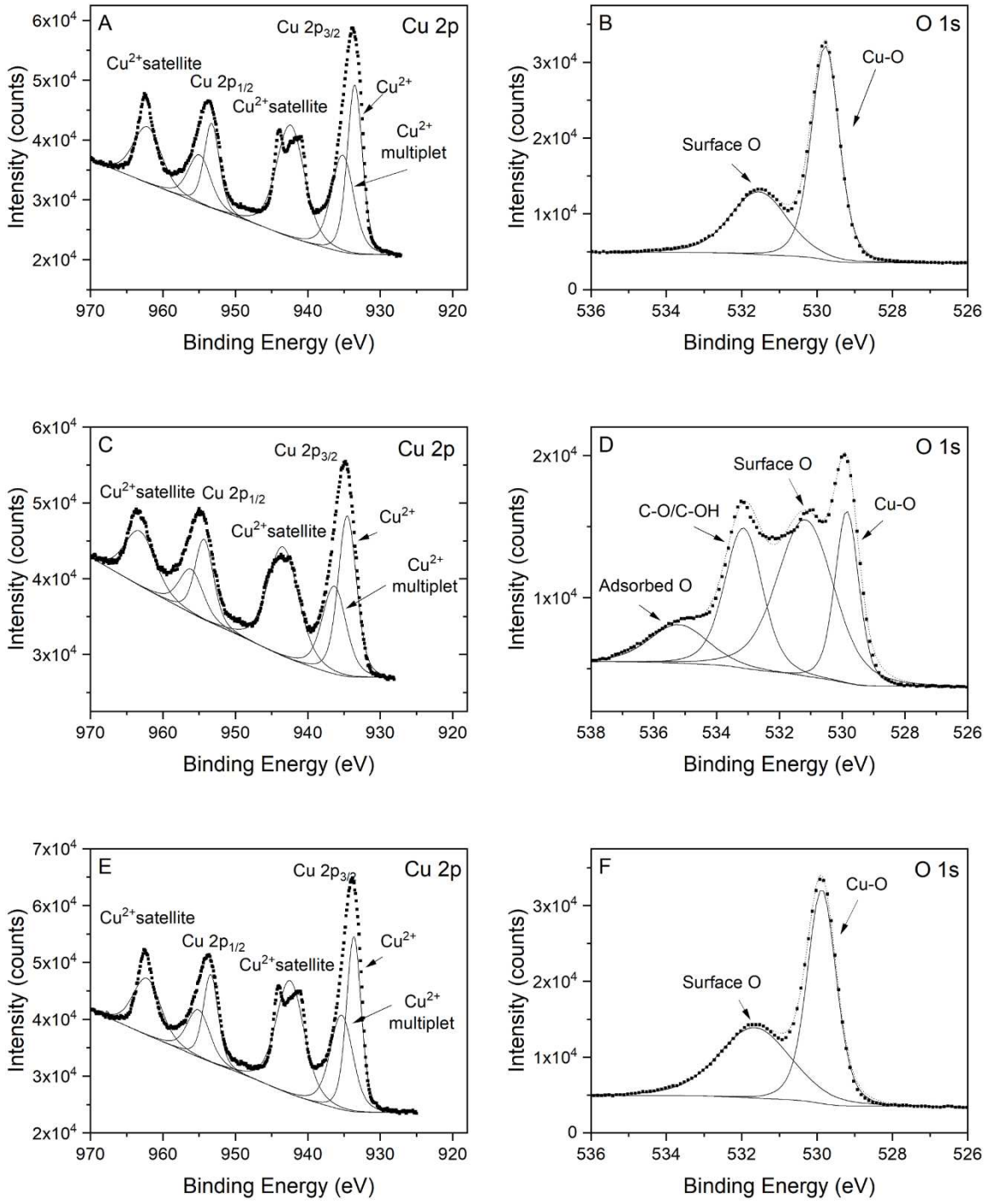

1197

1198 *Figure 3: High resolution XPS spectra of pristine CuO-L-3 (A, B), GO-CuO-L-3 (C, D), and*
1199 *rGO-CuO-L-3 (E, F) nanocomposites: Cu 2p spectra are shown in panels A, C, and E, while O*
1200 *1s spectra are shown in panels B, D, and F.*

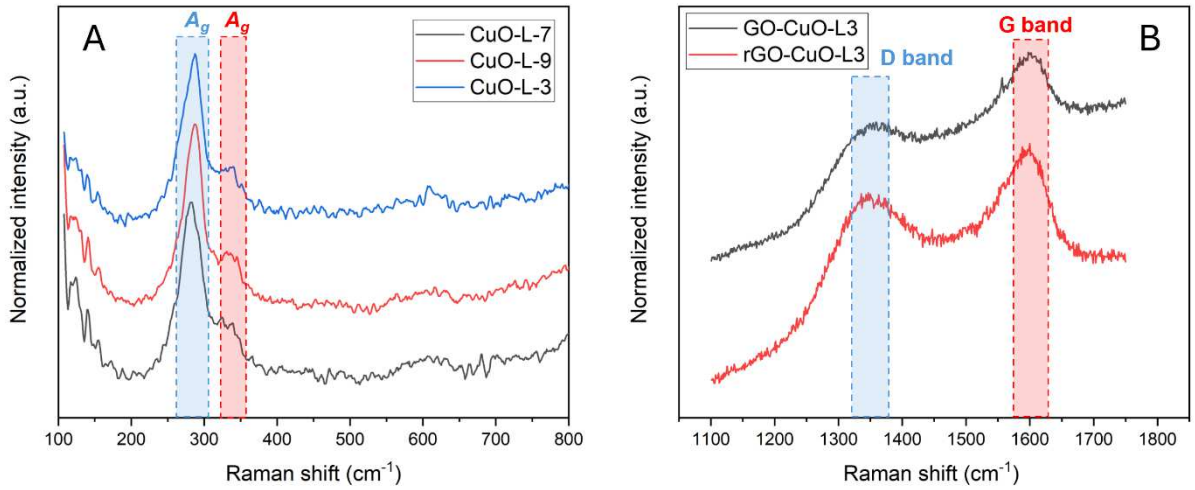

Figure 4 Raman spectra of (A) CuO NPs calcined at 200 (CuO-L-7), 300 (CuO-L-9), and 400 °C (CuO-L-3) and (B) GO-CuO-L-3 and rGO-CuO-L-3 nanocomposites calcined at 400 °C. In panel B, the spectra are shown in the 1100–1750 cm^{-1} region and were normalized to the G-band intensity (G = 1) to facilitate comparison of the D and G bands. The GO-CuO spectrum was vertically offset for clarity.

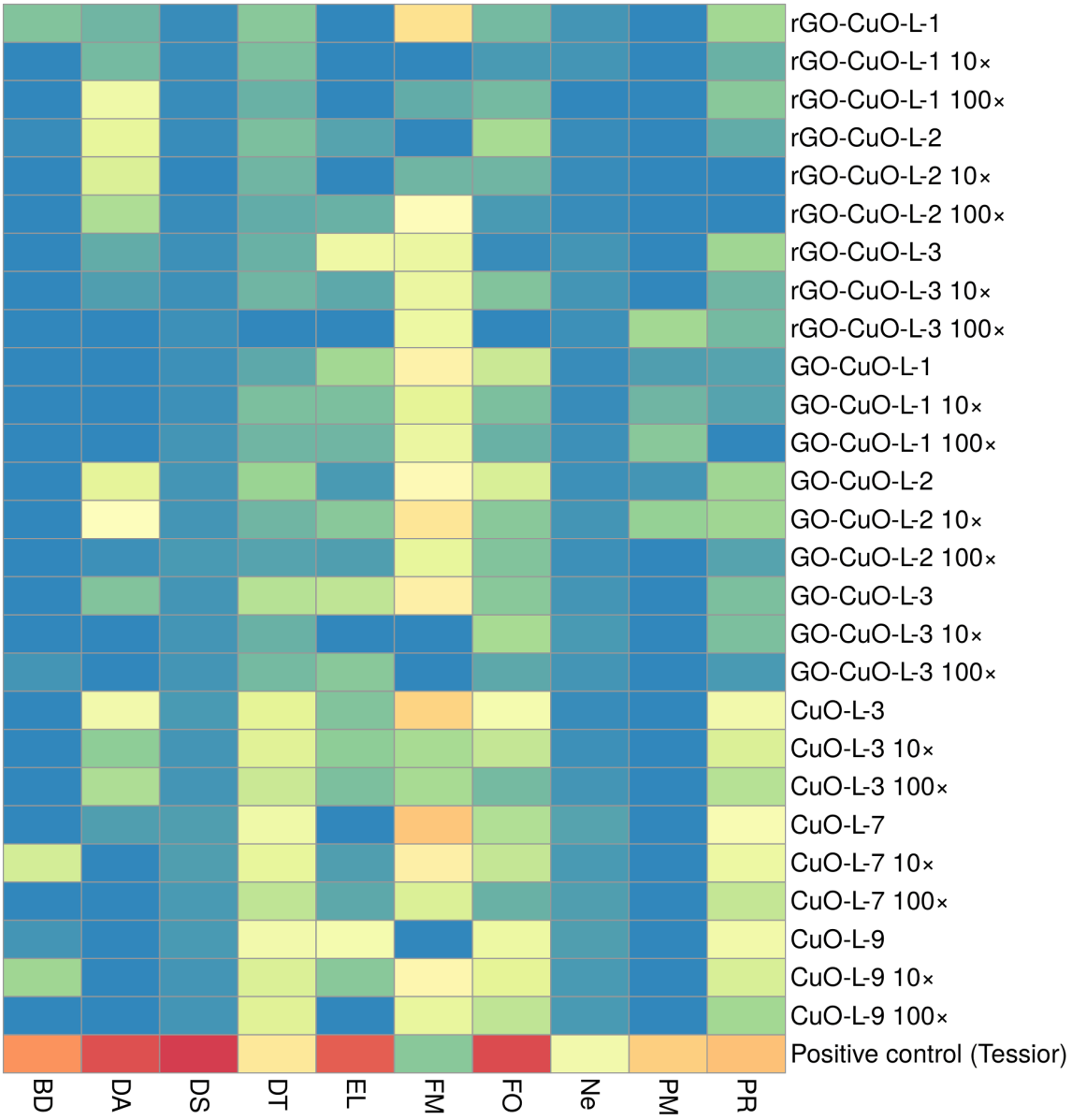

Figure 5: Heatmap illustrating pathogen-specific inhibition patterns of grapevine trunk disease-associated fungi following treatment with copper-based NPs. The negative control (sterile water) was omitted because no inhibition was observed for any pathogen. BD – B. dothidea, DT – D. torresensis, DA – D. ampelina, DS – D. seriata, EL – E. lata, FM – F. mediterranea, FO – F. oxysporum, Ne – Neonectria sp., PM – P. minimum, PR – P. richardsiae

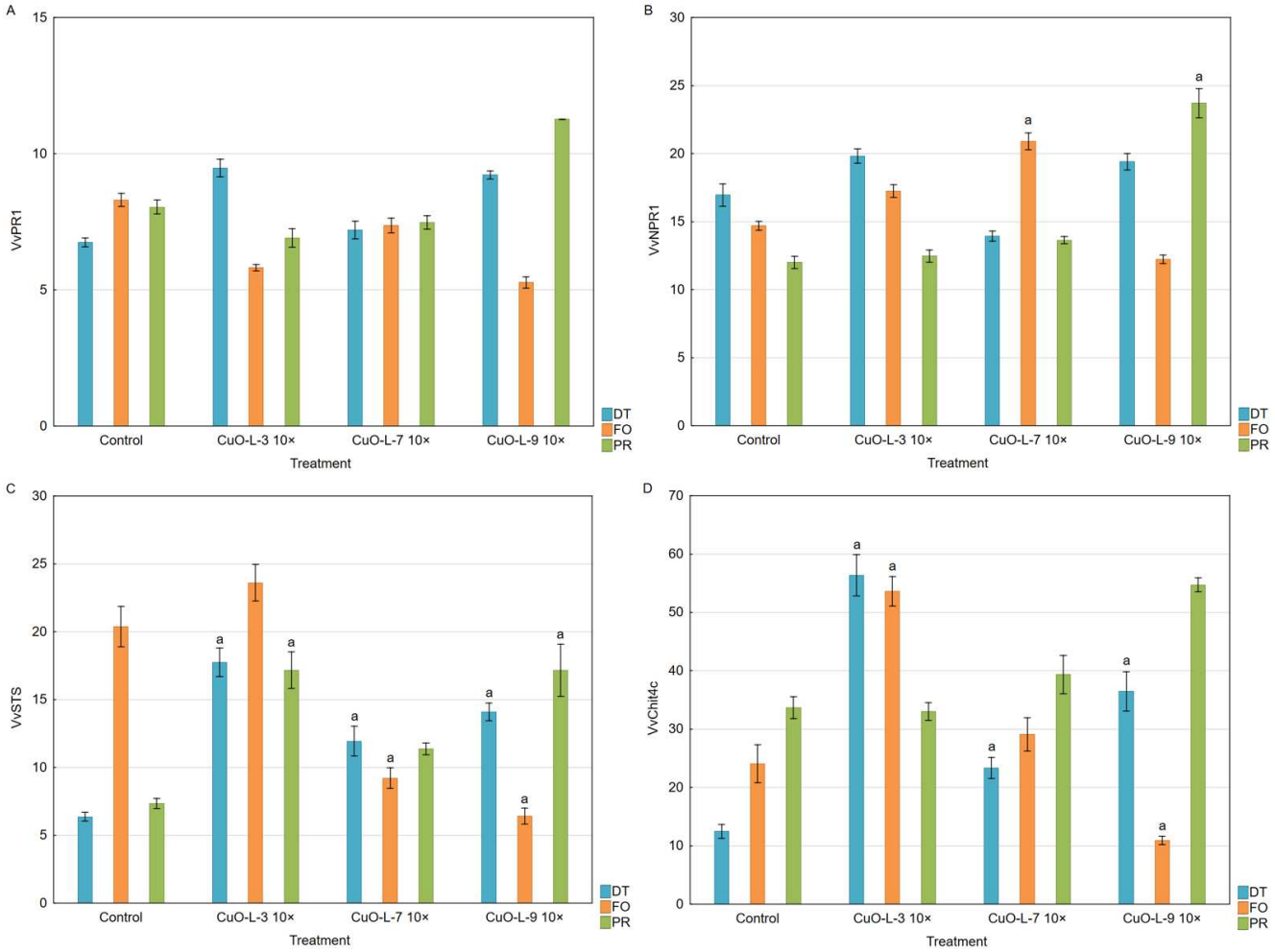

Figure 6: Expression levels of selected genes in grapevine seedlings inoculated with GTD pathogens and treated with CuO NPs. A – pathogenesis-related protein 1 (VvPR1), B – non-expresser of pathogenesis-related gene 1 (VvNPR1), C – stilbene synthase (VvSTS), D – acidic class IV chitinase (VvChit4c). DT – D. torresensis, FO – F. oxysporum, PR – P. richardsiae; a – statistically significant difference compared with the control ($p < 0.05$).

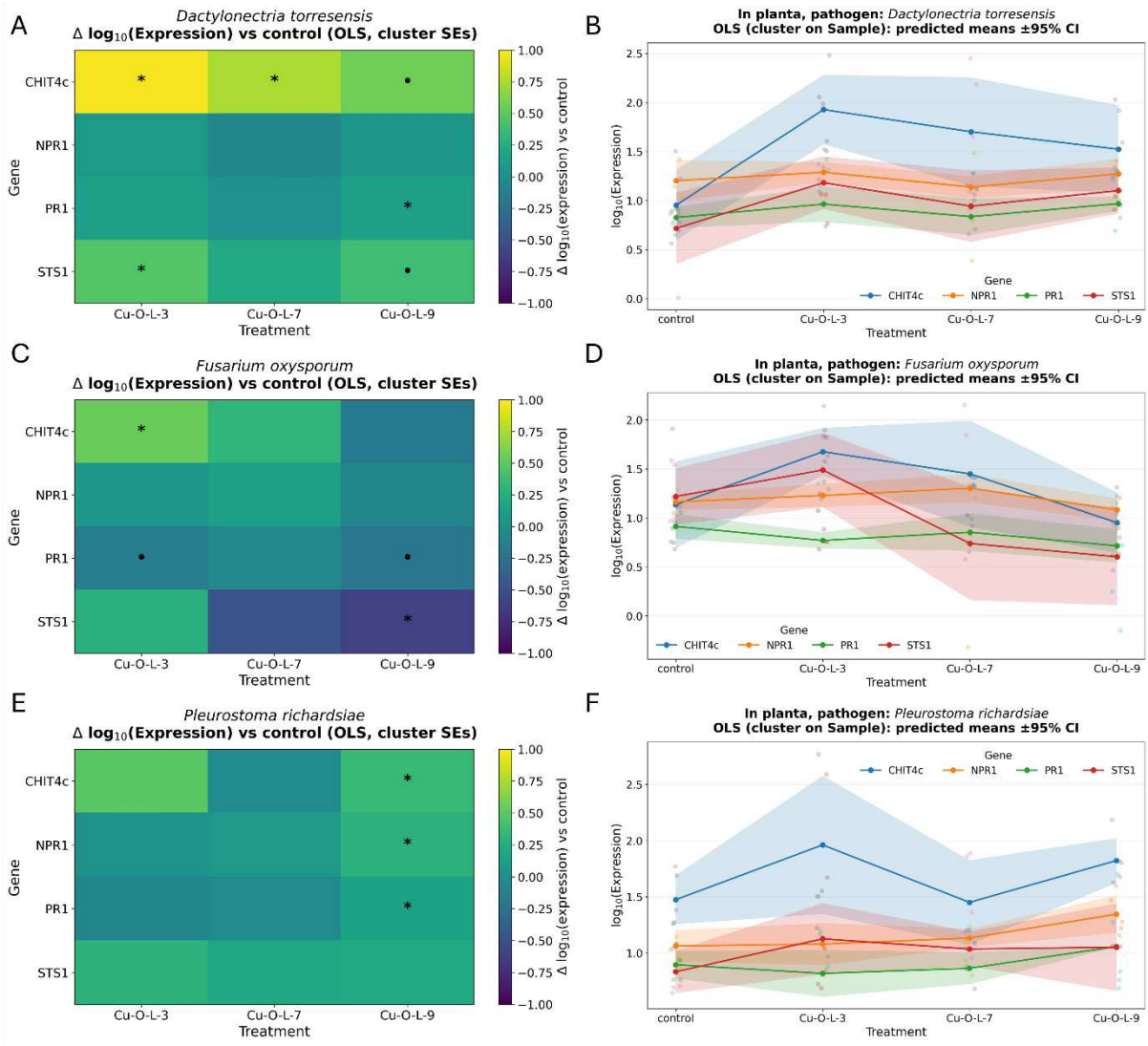

Figure 7: Pathogen-specific modulation of grapevine defence-related gene expression following CuO NP treatments. Heatmaps (A, C, E) show differences in log₁₀-transformed normalized gene expression relative to untreated controls estimated by OLS regression models. Positive values indicate increased expression relative to the control, whereas negative values indicate reduced expression. Symbols denote statistically significant differences from the untreated control ($p < 0.05$). Line plots (B, D, F) present OLS-predicted mean log₁₀-transformed expression values ± 95% confidence intervals for plants inoculated with D. torresensis (A, B), F. oxysporum (C, D), and P. richardsiae (E, F). VvPR1 – pathogenesis-related protein 1, VvNPR1 – non-expresser of pathogenesis-related gene 1, VvSTS – stilbene synthase, VvChit4c – acidic class IV chitinase.

Supplementary Files

This is a list of supplementary files associated with this preprint. Click to download.

- Additionalfile1.xlsx